

Electron–Photon Spatial Entanglement in Coherent Cathodoluminescence

Tatsuro Yuge,^{1,*} Ryo Okamoto,² Takumi Sannomiya,³ and Keiichirou Akiba^{4,†}

¹*Department of Physics, Shizuoka University, Shizuoka 422-8529, Japan*

²*Department of Electronic Science and Engineering, Kyoto University, Kyotodaigakukatsura, Nishikyo-ku, Kyoto 615-8510, Japan*

³*Department of Materials Science and Engineering, School of Materials and Chemical Technology, Institute of Science Tokyo, Kanagawa, 4259 Nagatsuta, Midori-ku 226-8503, Yokohama Japan*

⁴*Takasaki Institute for Advanced Quantum Science, National Institutes for Quantum Science and Technology, 1233 Watanuki, Takasaki, Gunma 370-1292, Japan*

Electron–photon quantum entanglement in an electron microscope paves the way for a new quantum platform, enabling the integration of quantum functionalities into electron microscopy and opening opportunities for quantum imaging and quantum sensing at the nanoscale. To realize such a platform, it is crucial to understand the degree and nature of electron–photon entanglement in cathodoluminescence (CL). However, its dependence on electron-beam properties, particularly transverse coherence, remains unclear. Here, we present a theoretical framework describing the quantum state of an electron–photon pair generated in coherent CL, specifically for transition radiation. By expressing the scattered state directly via the luminescence spectrum, we evaluate the entanglement using both subsystem purity and an Einstein-Podolsky-Rosen-type criterion. These two measures enable a clear distinction between wave-like, particle-like, and classical regimes in terms of spatial and momentum entanglement in the electron–photon system. Our analysis identifies the roles of the electron’s transverse and longitudinal coherence, as well as the photon’s spectral width, and reveals the conditions under which strong spatial entanglement emerges. This unified perspective clarifies the nature of electron–photon quantum correlations in coherent CL, leading to quantum-enabled functionalities in electron microscopy.

I. INTRODUCTION

Exploiting the wave nature of electrons, electron microscopy provides nanoscale visualization of materials combined with spectroscopic access to local material information such as elemental composition and electronic structure. The decisive experimental demonstration of the Aharonov-Bohm effect was enabled by the phase coherence of electron waves [1]. The Young’s double-slit experiment in electron microscopy successfully captured the single-electron buildup process of the interference pattern, excellently demonstrating the wave-particle duality of a single electron [2]. Thus, quantum features in electron microscopy are fundamentally rooted in the wave nature of electrons.

Recent advances have brought about novel quantum aspects of swift electrons, necessitating the frameworks of quantum electrodynamics and quantum optics [3, 4]. In such a framework, unprecedented technologies have been cultivated so far, including quantum-enhanced sensing and metrology beyond classical limits [5–8], as well as quantum computation and information processing [9–11]. Extending these concepts to electron microscopy offers novel opportunities for advancing its capabilities.

Indeed, this field of free-electron quantum optics is emerging, and electron systems in electron microscopy

can serve as a new quantum platform, where the coherent interaction between electrons and photons is crucial for their realization [3, 12]. Such electron–photon interactions in the quantum regime can also be exploited to advance nanophotonics [4, 13]. Pioneering studies have demonstrated that free electrons can be induced to emit and absorb integer numbers of photons through their interaction with laser fields [14]. Subsequently, the coherent quantum state manipulation of free-electron populations has been realized via strong light fields [15]. These experimental results advanced the quantum description of electron–photon interactions. Theoretical studies have widely investigated the quantum aspect of scattering and generation of entanglement between an electron and a photon [16–25]. In experimental studies, correlated electron–photon pairs have been demonstrated in transmission electron microscopes integrated with photonic systems, via cavity-mediated interaction [26] and via interaction with a membrane [27]. Only recently have demonstrations of electron–photon entanglement generated via cathodoluminescence (CL) been reported [28, 29].

These results mark a milestone in leveraging the unique quantum properties in electron microscopy. The introduction of quantum imaging techniques holds great potential for overcoming the critical issue of electron-beam induced damage [30, 31]. It is also expected that nonclassical light, which has not been achieved through conventional optical means, can be generated; for instance, unprecedented high-NOON states at megahertz rates [32]. Furthermore, theoretical investigations have proposed a

* yuge.tatsuro@shizuoka.ac.jp

† akiba.keiichiro@qst.go.jp

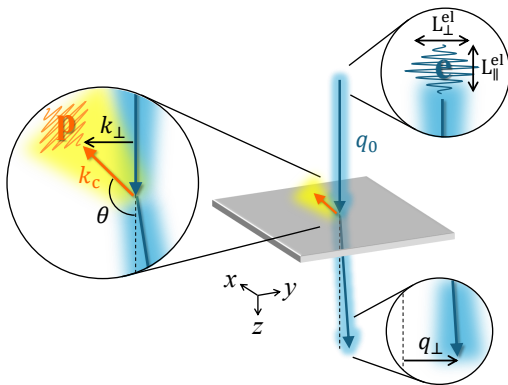


FIG. 1. Illustration of coherent cathodoluminescence in transition radiation. The wave packet of an incident electron has central momentum $\hbar q_0$ in the z direction with the spatial widths L_{\perp}^{el} and $L_{\parallel}^{\text{el}}$ in the transverse (xy) and longitudinal (z) directions, respectively. A photon in the radiation has a central wavenumber k_c (wavelength $\lambda_c = 2\pi/k_c$) in the direction of θ with the spectral width $\Delta\lambda_{\text{ph}}$. The electron undergoes a recoil to gain transverse momentum $\hbar q_{\perp}$.

variety of intriguing concepts for quantum information processing and quantum sensing [3, 33, 34]. Towards these advances, methods for achieving strong coupling between electrons and photons have been investigated [35–37]. However, the degree and nature of electron–photon entanglement in CL are not fully understood. It remains unclear how the entanglement depends on electron beam and optical emission properties, especially on the transverse coherence of the electron beam. Moreover, different entanglement measures may give qualitatively different assessments of the entangled state, and a systematic understanding of these differences is still lacking.

In this paper, we identify the physical conditions under which distinct forms of electron–photon entanglement arise in transition radiation (schematically illustrated in Fig. 1), a representative coherent CL process. We show that the scattered state exhibits three distinct entanglement regimes, as shown in Fig. 2(a): two of them (A and B) correspond to different types of entangled states, while the third (C) is a non-entangled regime. We further demonstrate that these regimes correspond to the wave-like, particle-like, and classical regimes recently proposed in Ref. [21] for electron–energy–photon–number entanglement, thereby extending these concepts to spatial and momentum entanglement. By clarifying the conditions under which strong electron–photon entanglement can be realized, our results provide a unified perspective on quantum correlations in CL and offer practical guidelines for generating spatially entangled electron–photon pairs.

To achieve this, we develop a theoretical framework to reconstruct the scattered state $|\Psi_{\text{sc}}\rangle$ of electron–photon pairs directly from the CL spectrum. This framework assumes translational symmetry in the plane perpendicular to the electron beam, a condition typically realized in transition radiation (Fig. 1). Within this approach,

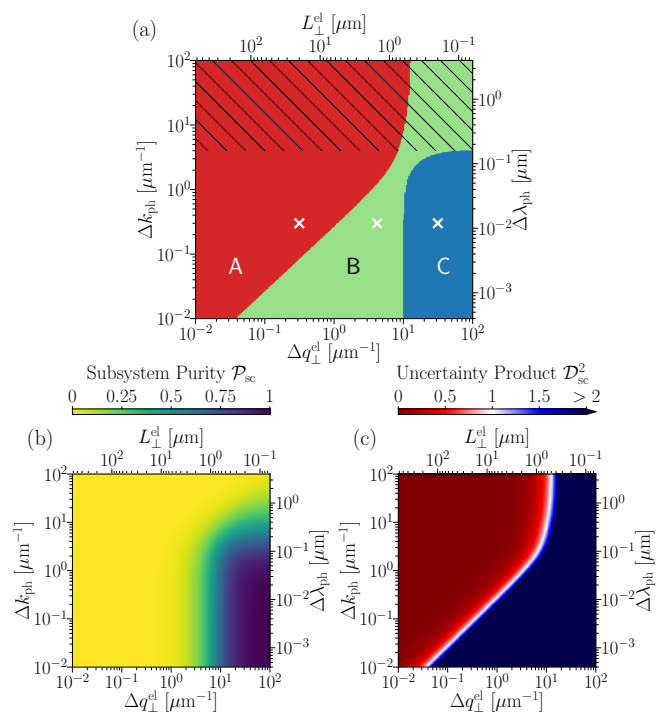


FIG. 2. (a) Parameter regimes of entanglement in the scattered state $|\Psi_{\text{sc}}\rangle$ (Sec. III) of the electron–photon system. Regimes A (red), B (light green), and C (blue) are defined based on (b) subsystem purity \mathcal{P}_{sc} (Sec. IV A) and (c) uncertainty product $\mathcal{D}_{\text{sc}}^2$ (Sec. IV B). Regime A corresponds to the wave-like entangled regime, where $\mathcal{P}_{\text{sc}} < 2/3$ and $\mathcal{D}_{\text{sc}}^2 < 1$; Regime B to the particle-like entangled regime, where $\mathcal{P}_{\text{sc}} < 2/3$ and $\mathcal{D}_{\text{sc}}^2 > 1$; and Regime C to the classical regime, where $\mathcal{P}_{\text{sc}} > 2/3$ and $\mathcal{D}_{\text{sc}}^2 > 1$. The upper hatched region indicates the entangled regime identified by the electron z -subsystem purity $\mathcal{P}_z^{\text{el}} < 2/3$, i.e., entanglement between the electron’s z -degree of freedom and the remaining degrees of freedom (Sec. IV D). We note that the subsystem purities \mathcal{P}_{sc} and $\mathcal{P}_z^{\text{el}}$ do not provide a strict threshold for entanglement; here, we adopt $2/3$ as a practical threshold. The qualitative features in (a) remain unchanged even if this threshold is chosen closer to unity. The horizontal and vertical axes represent the transverse width of the electron wavenumber $\Delta q_{\perp}^{\text{el}}$ and the luminescence spectral width Δk_{ph} , respectively. The parameters are $K = 200$ keV, $\lambda_c = 0.5 \mu\text{m}$, and $L_{\parallel}^{\text{el}} = 1.3 \mu\text{m}$.

we quantify entanglement using the subsystem purity and the EPR (Einstein-Podolsky-Rosen) criterion [see Figs. 2(b) and (c)].

The paper is organized as follows. Section II introduces a theoretical model for electron–photon interactions in coherent CL and outlines the assumptions underlying our framework. Section III presents an expression for the scattered electron–photon state $|\Psi_{\text{sc}}\rangle$ reconstructed from the luminescence spectrum. Section IV provides a quantitative analysis of electron–photon entanglement using the two measures. We identify wave-like, particle-like, and classical regimes and clarify the roles of the transverse and longitudinal electron coherence, as well as the

CL spectral width. We also present the joint probability distributions of the relative position and total wavevector in the electron–photon state. Finally, Sec. V summarizes our results and provides their implications.

II. ELECTRON–PHOTON INTERACTION

We consider coherent CL, focusing in particular on transition radiation generated by an incident electron beam [38]. As illustrated in Fig. 1, an electron beam along the z direction impinges on a planar sample in the xy plane. When an electron in the beam enters the sample, optical excitations are induced and subsequently radiative emission occurs. The emitted electromagnetic field, in turn, exerts a recoil on the electron. In this work, we focus on the weak-coupling regime, in which each electron induces either zero- or one-photon emission.

Within this setup, we analyze the scattering process between a single electron in the beam and the radiation field. The total Hamiltonian of the electron–photon system $\hat{H} = \hat{H}_0 + \hat{H}_{\text{int}}$ is composed of the free Hamiltonian $\hat{H}_0 = \hat{\mathbf{p}}^2/(2m) + \sum_{\mathbf{k}} \hbar\omega_{\mathbf{k}} \hat{a}_{\mathbf{k}}^\dagger \hat{a}_{\mathbf{k}}$ and the electron–photon interaction \hat{H}_{int} . Here $\hat{\mathbf{p}}$ is the momentum operator of the electron, m is the electron mass, and $\hat{a}_{\mathbf{k}}$ ($\hat{a}_{\mathbf{k}}^\dagger$) is the annihilation (creation) operator of a photon with a wavevector \mathbf{k} . The photon frequency is given by $\omega_{\mathbf{k}} = ck$, where $k = |\mathbf{k}|$ and c is the speed of light.

In this work, we assume that the electron–photon system is translationally invariant in the transverse (xy) plane perpendicular to the electron beam and rotationally symmetric around the beam axis. In the context of CL, this situation is typically realized in transition radiation (Fig. 1), where the transverse extent of the sample is sufficiently large. The translational invariance in the transverse plane implies that the in-plane momentum of the electron–photon system is conserved in the scattering process. Consequently, the interaction Hamiltonian \hat{H}_{int} takes the form

$$\langle \mathbf{q}, \mathbf{k} | \hat{H}_{\text{int}} | \mathbf{q}', \text{vac} \rangle = h(\mathbf{k}, q_z - q'_z) \delta(\mathbf{q}_\perp + \mathbf{k}_\perp - \mathbf{q}'_\perp), \quad (1)$$

where $\mathbf{q} = (q_x, q_y, q_z)$ and $\mathbf{k} = (k_x, k_y, k_z)$ are the wavevectors of the electron and photon, respectively, and $\mathbf{q}_\perp = (q_x, q_y)$ and $\mathbf{k}_\perp = (k_x, k_y)$ denote their transverse components. The function $h(\mathbf{k}, q_z - q'_z)$ represents the interaction strength. The states appearing in Eq. (1) are defined as follows: $|\mathbf{q}', \text{vac}\rangle = |\mathbf{q}'\rangle_{\text{el}} |\text{vac}\rangle_{\text{ph}}$ and $|\mathbf{q}, \mathbf{k}\rangle = |\mathbf{q}\rangle_{\text{el}} |\mathbf{k}\rangle_{\text{ph}}$, where $|\mathbf{q}\rangle_{\text{el}}$ is the eigenstate of $\hat{\mathbf{p}}$ satisfying $\hat{\mathbf{p}}|\mathbf{q}\rangle_{\text{el}} = \hbar\mathbf{q}|\mathbf{q}\rangle_{\text{el}}$, $|\text{vac}\rangle_{\text{ph}}$ is the photon vacuum state satisfying $\hat{a}_{\mathbf{k}}|\text{vac}\rangle_{\text{ph}} = 0$, and $|\mathbf{k}\rangle_{\text{ph}} = \hat{a}_{\mathbf{k}}^\dagger|\text{vac}\rangle_{\text{ph}}$ is a single-photon state. Furthermore, the rotational symmetry implies that the interaction strength satisfies $h(k_\perp \cos \phi, k_\perp \sin \phi, k_z, q_z - q'_z)$ being invariant under rotations $0 \leq \phi < 2\pi$.

III. SCATTERED STATE

We now analyze the quantum state of the electron–photon system generated by the scattering process. We consider an initial state consisting of a single-electron wave packet and the photon vacuum, $|\Psi_{\text{ini}}\rangle = \int d^3q \psi_{\text{ini}}(\mathbf{q}) |\mathbf{q}, \text{vac}\rangle$, where $\psi_{\text{ini}}(\mathbf{q})$ denotes the wavevector-space wave function of the incoming electron.

In the weak-coupling regime considered here, a perturbation analysis in \hat{H}_{int} [39] yields that the electron–photon state after the scattering can be written as $|\Psi_{\text{fin}}\rangle = \sqrt{1-a}|\Psi_0\rangle + \sqrt{a}|\Psi_{\text{sc}}\rangle$ ($0 < a < 1$). Here $|\Psi_0\rangle = \int d^3q \psi_0(\mathbf{q}) |\mathbf{q}, \text{vac}\rangle$ is a state that has no generated photons and $|\Psi_{\text{sc}}\rangle$ is the scattered state associated with single-photon generation (see Appendix A 1 for the detailed derivation including the form of $\psi_0(\mathbf{q})$).

Furthermore, using the interaction matrix element given in Eq. (1), we find that $|\Psi_{\text{sc}}\rangle$ can be reconstructed from the excitation probability density $\Gamma(\mathbf{k})$ of a photon with \mathbf{k} as (see Appendix A 2 for the detailed derivation)

$$|\Psi_{\text{sc}}\rangle = \int d^3q d^3k \psi_{\text{sc}}(\mathbf{q}, \mathbf{k}) |\mathbf{q}, \mathbf{k}\rangle, \quad (2)$$

$$\psi_{\text{sc}}(\mathbf{q}, \mathbf{k}) = \psi_{\text{ini}}(\mathbf{q}_\perp + \mathbf{k}_\perp, q_z + ck/v_z) \sqrt{\Gamma(\mathbf{k})} e^{i\eta(\mathbf{k})}. \quad (3)$$

In this equation, $\psi_{\text{ini}}(\mathbf{q}_\perp, q_z)$ denotes $\psi_{\text{ini}}(\mathbf{q})$ with $\mathbf{q} = (\mathbf{q}_\perp, q_z)$ and $\mathbf{q}_\perp = (q_x, q_y)$. Here, v_z is the mean velocity of an incident electron and $\eta(\mathbf{k})$ is an undetermined phase that cannot be inferred from the luminescence spectrum $\Gamma(\mathbf{k})$ alone and that may depend on \mathbf{k} . We note that the phase $\eta(\mathbf{k})$ can be eliminated by a local operation on the photon.

This formulation can be straightforwardly extended to the case where a filter is applied to the photon. Indeed, when a photonic filter with a transfer function $F(\mathbf{k})$ is applied to the scattered state $|\Psi_{\text{sc}}\rangle$, the filtered state, $|\tilde{\Psi}_{\text{sc}}\rangle = \sqrt{\mathcal{N}_F} \int d^3k F(\mathbf{k}) |\mathbf{k}\rangle_{\text{ph}} \langle \mathbf{k} | \Psi_{\text{sc}} \rangle$ with $\mathcal{N}_F^{-1} = \int d^3k |F(\mathbf{k})|^2 \Gamma(\mathbf{k})$, can be written as $|\tilde{\Psi}_{\text{sc}}\rangle = \int d^3q d^3k \tilde{\psi}_{\text{sc}}(\mathbf{q}, \mathbf{k}) |\mathbf{q}, \mathbf{k}\rangle$, where

$$\tilde{\psi}_{\text{sc}}(\mathbf{q}, \mathbf{k}) = \psi_{\text{ini}}(\mathbf{q}_\perp + \mathbf{k}_\perp, q_z + ck/v_z) F(\mathbf{k}) \sqrt{\mathcal{N}_F \Gamma(\mathbf{k})} e^{i\eta(\mathbf{k})}. \quad (4)$$

By introducing the redefined quantities $\tilde{\Gamma}(\mathbf{k}) = \mathcal{N}_F |F(\mathbf{k})|^2 \Gamma(\mathbf{k})$ and $e^{i\tilde{\eta}(\mathbf{k})} = e^{i\eta(\mathbf{k})} F(\mathbf{k})/|F(\mathbf{k})|$, the filtered state $|\tilde{\Psi}_{\text{sc}}\rangle$ can be cast into the same form as Eqs. (2) and (3). Hereafter, $\Gamma(\mathbf{k})$ and $\eta(\mathbf{k})$ are therefore understood to represent either the original or their filtered quantities, depending on the context.

In the following, we assume that the initial electron wave function $\psi_{\text{ini}}(\mathbf{q})$ has a Gaussian form: $\psi_{\text{ini}}(\mathbf{q}) = \prod_{\alpha=x,y,z} \psi_{\text{ini}}^{(\alpha)}(q_\alpha)$, where

$$\psi_{\text{ini}}^{(\alpha)}(q_\alpha) = \frac{1}{(2\pi)^{1/4} (\Delta q_\perp^{\text{el}})^{1/2}} \exp\left[-\frac{q_\alpha^2}{4(\Delta q_\perp^{\text{el}})^2}\right] \quad (5)$$

for $\alpha = x, y$, and

$$\psi_{\text{ini}}^{(z)}(q_z) = \frac{1}{(2\pi)^{1/4}(\Delta q_{\parallel}^{\text{el}})^{1/2}} \exp\left[-\frac{(q_z - q_0)^2}{4(\Delta q_{\parallel}^{\text{el}})^2}\right]. \quad (6)$$

This means that the electron has, on average, a wavevector $(0, 0, q_0)$, with an uncertainty width of $\Delta q_{\perp}^{\text{el}}$ in the transverse (xy) direction and $\Delta q_{\parallel}^{\text{el}}$ in the longitudinal (z) direction. The central wavenumber q_0 is determined by the electron kinetic energy K as $\hbar q_0 = (1/c)\sqrt{K^2 + 2mc^2K}$ and is related to the mean velocity as $v_z = \hbar q_0/m$. $\Delta q_{\perp}^{\text{el}}$ and $\Delta q_{\parallel}^{\text{el}}$ are estimated from the transverse and longitudinal coherence lengths of the electron beam as $\Delta q_{\perp}^{\text{el}} = 2\pi/L_{\perp}^{\text{el}}$ and $\Delta q_{\parallel}^{\text{el}} = 2\pi/L_{\parallel}^{\text{el}}$, respectively.

Furthermore, for an illustrative calculation, we assume a model for the luminescence spectrum $\Gamma(\mathbf{k})$. Owing to the rotational symmetry in the transverse plane, $\Gamma(\mathbf{k})$ is independent of the azimuthal angle ϕ . We further assume that the photon wavenumber k of the luminescence is peaked around k_c with a characteristic width Δk_{ph} , and that the photon emission is strongest in the directions with polar angles $\theta = \pi/4$ and $3\pi/4$, as characteristic of transition radiation. Specifically, we adopt the following form of $\Gamma(\mathbf{k})$ in the spherical coordinates:

$$\Gamma(\mathbf{k}) = \Gamma(k, \theta, \phi) = g(k)f(\theta), \quad (7)$$

$$g(k) = \mathcal{N}_g \exp\left[-\frac{(k - k_c)^2}{2\Delta k_{\text{ph}}^2}\right], \quad (8)$$

$$f(\theta) = \frac{15}{8\pi}(\sin\theta \cos\theta)^2. \quad (9)$$

The normalization constant \mathcal{N}_g for $g(k)$ is defined to satisfy $\int_0^{\infty} dk k^2 g(k) = 1$, so that

$$\begin{aligned} \mathcal{N}_g^{-1} &= \sqrt{\frac{\pi}{2}} \Delta k_{\text{ph}} (\Delta k_{\text{ph}}^2 + k_c^2) \left[\text{erf}\left(\frac{k_c}{\sqrt{2}\Delta k_{\text{ph}}}\right) + 1 \right] \\ &+ k_c \Delta k_{\text{ph}}^2 \exp\left(-\frac{k_c^2}{2\Delta k_{\text{ph}}^2}\right), \end{aligned} \quad (10)$$

where $\text{erf}(\cdot)$ is the Gauss error function. By this normalization, $\Gamma(\mathbf{k})$ is also normalized: $\int d\mathbf{k} \Gamma(\mathbf{k}) = \int dk d\theta d\phi k^2 \sin\theta \Gamma(k, \theta, \phi) = 1$. We note that k_c and Δk_{ph} are related to the central wavelength λ_c and the spectral width $\Delta\lambda_{\text{ph}}$ via $k_c = 2\pi/\lambda_c$ and $\Delta k_{\text{ph}} = 2\pi\Delta\lambda_{\text{ph}}/\lambda_c^2$, respectively. When a photonic bandpass filter is applied, λ_c and $\Delta\lambda_{\text{ph}}$ correspond to the central wavelength and bandwidth of the filter, respectively.

IV. ELECTRON-PHOTON ENTANGLEMENT

We now quantitatively evaluate the degree of electron-photon entanglement in the scattered state $|\Psi_{\text{sc}}\rangle$. Experimentally, $|\Psi_{\text{sc}}\rangle$ can be obtained by post-selecting single-photon emission events in $|\Psi_{\text{fin}}\rangle$. To characterize the entanglement, we employ two measures: (i) the

purity of the reduced density matrix of the electron, and (ii) the EPR-type correlation criterion for continuous-variable systems proposed in Ref. [40].

In the main illustrative evaluation shown in Fig. 2, we use the longitudinal coherence length $L_{\parallel}^{\text{el}} = 1.3 \mu\text{m}$ for the electron beam, which is typical for a field emission gun [41].

A. Subsystem purity

We first quantify the electron-photon entanglement using the subsystem purity of the scattered state, defined as

$$\mathcal{P}_{\text{sc}} = \text{Tr}_{\text{el}} \left[(\text{Tr}_{\text{ph}} |\Psi_{\text{sc}}\rangle\langle\Psi_{\text{sc}}|)^2 \right], \quad (11)$$

where Tr_{el} (Tr_{ph}) denotes the trace over the electron (photon) system. This quantity satisfies $0 \leq \mathcal{P}_{\text{sc}} \leq 1$, and $\mathcal{P}_{\text{sc}} = 1$ holds if and only if $|\Psi_{\text{sc}}\rangle$ is separable between the electron and photon. The inverse of the subsystem purity, $K_{\text{Schmidt}} = 1/\mathcal{P}_{\text{sc}}$, corresponds to the Schmidt number, which is widely used to quantify entanglement in continuous-variable bipartite pure states [42–50]. K_{Schmidt} represents the effective number of coefficients in the Schmidt decomposition of $|\Psi_{\text{sc}}\rangle$. Thus, a larger K_{Schmidt} indicates that a greater number of modes significantly contribute to the entanglement in $|\Psi_{\text{sc}}\rangle$. In this sense, a lower \mathcal{P}_{sc} signals a higher degree of entanglement. We note that the subsystem purity does not provide a strict threshold for entanglement. We adopt $2/3$ as a practical threshold in the classification shown in Fig. 2(a). The qualitative features in Fig. 2(a), as well as the conclusions, remain unchanged even if this threshold is chosen closer to unity.

Using Eqs. (2) and (3) for $|\Psi_{\text{sc}}\rangle$ with Eqs. (5) and (6) for ψ_{ini} , we find that \mathcal{P}_{sc} is given by

$$\begin{aligned} \mathcal{P}_{\text{sc}} &= \int d^3k d^3k' \Gamma(\mathbf{k})\Gamma(\mathbf{k}') \\ &\times \exp\left[-\frac{|\mathbf{k}_{\perp} - \mathbf{k}'_{\perp}|^2}{4(\Delta q_{\perp}^{\text{el}})^2} - \frac{c^2(k - k')^2}{4v_z^2(\Delta q_{\parallel}^{\text{el}})^2}\right]. \end{aligned} \quad (12)$$

We note that this is independent of the undetermined phase $\eta(\mathbf{k})$. The derivation of this result is given in Appendix B.

We evaluate \mathcal{P}_{sc} by substituting the model for $\Gamma(\mathbf{k})$ [Eqs. (7)–(9)] into the above expression and numerically computing the integral. In Fig. 2(b), we show a color plot of \mathcal{P}_{sc} as a function of $\Delta q_{\perp}^{\text{el}}$ and Δk_{ph} (L_{\perp}^{el} and $\Delta\lambda_{\text{ph}}$) for the case of $L_{\parallel}^{\text{el}} = 1.3 \mu\text{m}$ ($\Delta q_{\parallel}^{\text{el}} \simeq 4.83 \mu\text{m}^{-1}$) and $\lambda_c = 0.5 \mu\text{m}$ ($k_c \simeq 12.6 \mu\text{m}^{-1}$). We find that $\mathcal{P}_{\text{sc}} \simeq 1$ in the region satisfying $\Delta q_{\perp}^{\text{el}} \gtrsim 20 \mu\text{m}^{-1}$ ($L_{\perp}^{\text{el}} \lesssim 0.3 \mu\text{m}$) and $\Delta k_{\text{ph}} \lesssim 2 \mu\text{m}^{-1}$ ($\Delta\lambda_{\text{ph}} \lesssim 0.1 \mu\text{m}$), whereas $\mathcal{P}_{\text{sc}} \simeq 0$ far outside of this region. The latter indicates that essentially an unbounded number of Schmidt modes contribute to the entanglement, which is characteristic of

entangled states in continuous-variable systems. This result shows that strong electron–photon entanglement is realized when L_{\perp}^{el} exceeds several micrometers.

B. EPR correlation

We next analyze the electron–photon entanglement in the x direction in the scattered state $|\Psi_{\text{sc}}\rangle$ using the criterion proposed in Ref. [40], which is employed to detect EPR correlations in continuous-variable systems [51–53]. In the context of the present electron–photon system, this criterion is based on the x -directional uncertainty product of the relative position, $x_{\text{el}} - x_{\text{ph}}$, and the total wavevector, $q_x^{\text{el}} + k_x^{\text{ph}}$:

$$\mathcal{D}_{\text{sc}}^2 = \langle [\Delta(x_{\text{el}} - x_{\text{ph}})]^2 \rangle \langle [\Delta(q_x^{\text{el}} + k_x^{\text{ph}})]^2 \rangle. \quad (13)$$

Here the expectation values are taken in the scattered state $|\Psi_{\text{sc}}\rangle$. The criterion states that $\mathcal{D}_{\text{sc}}^2 \geq 1$ if $|\Psi_{\text{sc}}\rangle$ is separable between the electron and photon; thus, $\mathcal{D}_{\text{sc}}^2 < 1$ indicates the electron–photon entanglement. Indeed, this type of criterion was recently used in the verification of electron–photon entanglement [28].

Using Eqs. (2) and (3) for $|\Psi_{\text{sc}}\rangle$ with Eqs. (5) and (6) for ψ_{ini} , we find that the relative position uncertainty is given by

$$\begin{aligned} & \langle [\Delta(x_{\text{el}} - x_{\text{ph}})]^2 \rangle \\ &= \frac{1}{8} \int d^3k \left\{ \frac{1}{\Gamma(\mathbf{k})} \left[\left(\frac{\partial \Gamma(\mathbf{k})}{\partial k_x} \right)^2 + \left(\frac{\partial \Gamma(\mathbf{k})}{\partial k_y} \right)^2 \right] \right. \\ & \quad \left. - 2 \left(\frac{\partial^2 \Gamma(\mathbf{k})}{\partial k_x^2} + \frac{\partial^2 \Gamma(\mathbf{k})}{\partial k_y^2} \right) + \frac{c^2 k_{\perp}^2 \Gamma(\mathbf{k})}{v_z^2 (\Delta q_{\parallel}^{\text{el}})^2 k^2} \right\} \\ & \quad + \frac{1}{2} \int d^3k \Gamma(\mathbf{k}) \left[\left(\frac{\partial \eta(\mathbf{k})}{\partial k_x} \right)^2 + \left(\frac{\partial \eta(\mathbf{k})}{\partial k_y} \right)^2 \right], \quad (14) \end{aligned}$$

and the total wavevector uncertainty is given by

$$\langle [\Delta(q_x^{\text{el}} + k_x^{\text{ph}})]^2 \rangle = (\Delta q_{\perp}^{\text{el}})^2. \quad (15)$$

We note that $\langle [\Delta(q_x^{\text{el}} + k_x^{\text{ph}})]^2 \rangle$ is independent of both the undetermined phase $\eta(\mathbf{k})$ and the CL spectrum $\Gamma(\mathbf{k})$, whereas $\langle [\Delta(x_{\text{el}} - x_{\text{ph}})]^2 \rangle$ depends on them. The derivation of Eqs. (14) and (15) is given in Appendix D. The result in Eq. (15), showing $\langle [\Delta(q_x^{\text{el}} + k_x^{\text{ph}})]^2 \rangle$ is determined solely by the electron’s transverse coherence, can be understood from the translational invariance in the transverse plane. Since the total transverse momentum $\hbar \mathbf{q}_{\perp} + \hbar \mathbf{k}_{\perp}$ is conserved in this electron–photon system (i.e., the corresponding total transverse momentum operator commutes with $\hat{H} = \hat{H}_0 + \hat{H}_{\text{int}}$), its variance is also conserved and thus coincides with that of the initial state $|\Psi_{\text{ini}}\rangle$.

Using the model for $\Gamma(\mathbf{k})$ [Eqs. (7)–(9)], we further proceed with the calculation of $\langle [\Delta(x_{\text{el}} - x_{\text{ph}})]^2 \rangle$ to obtain

(see Appendix D 1 for the detailed derivation)

$$\begin{aligned} & \langle [\Delta(x_{\text{el}} - x_{\text{ph}})]^2 \rangle \\ &= \frac{\sqrt{2\pi} \mathcal{N}_g}{56} \left(19 \Delta k_{\text{ph}} + \frac{2k_c^2}{\Delta k_{\text{ph}}} \right) \left[\text{erf} \left(\frac{k_c}{\sqrt{2} \Delta k_{\text{ph}}} \right) + 1 \right] \\ & \quad + \frac{\mathcal{N}_g}{14} k_c \exp \left(-\frac{k_c^2}{2 \Delta k_{\text{ph}}^2} \right) + \frac{c^2}{14 v_z^2 (\Delta q_{\parallel}^{\text{el}})^2} + D_{\eta}, \quad (16) \end{aligned}$$

where $D_{\eta} = (1/2) \int d^3k \Gamma(\mathbf{k}) \sum_{\alpha=x,y} [\partial \eta(\mathbf{k}) / \partial k_{\alpha}]^2$. To discuss the entanglement intrinsic to the scattering state $|\Psi_{\text{sc}}\rangle$, it is sufficient to consider the case where the $\eta(\mathbf{k})$ -dependent term D_{η} is minimized, since the phase $\eta(\mathbf{k})$ in $|\Psi_{\text{sc}}\rangle$ can be changed by a local unitary transformation on the photon. In the following, we focus on the case where $D_{\eta} = 0$, which yields the minimum. In practical experiments, however, the effect of the phase $\eta(\mathbf{k})$ may not be perfectly eliminated; its influence on the uncertainty product $\mathcal{D}_{\text{sc}}^2$ is therefore discussed in Appendix E.

We evaluate the uncertainty product $\mathcal{D}_{\text{sc}}^2$ by multiplying Eqs. (15) and (16). In Fig. 2(c), we show a color plot of $\mathcal{D}_{\text{sc}}^2$ as a function of $\Delta q_{\perp}^{\text{el}}$ and Δk_{ph} (L_{\perp}^{el} and $\Delta \lambda_{\text{ph}}$) for the case of $L_{\parallel}^{\text{el}} = 1.3 \mu\text{m}$ ($\Delta q_{\parallel}^{\text{el}} \simeq 4.83 \mu\text{m}^{-1}$) and $\lambda_c = 0.5 \mu\text{m}$ ($k_c \simeq 12.6 \mu\text{m}^{-1}$). We find that $\mathcal{D}_{\text{sc}}^2$ is significantly smaller than one in the upper-left region of the plot. For instance, when $\Delta k_{\text{ph}} = 3 \mu\text{m}^{-1}$ ($\Delta \lambda_{\text{ph}} \simeq 0.01 \mu\text{m}$), L_{\perp}^{el} must exceed a few micrometers to achieve strong electron–photon EPR correlation in the x direction.

We also find that, along the line of $\mathcal{D}_{\text{sc}}^2 = 1$ shown in white in Fig. 2(c), $\Delta k_{\text{ph}} \propto \Delta q_{\perp}^{\text{el}}$ in the small- Δk_{ph} region [$\Delta k_{\text{ph}} \lesssim 1 \mu\text{m}^{-1}$; the unhatched regime in Fig. 2(a)], whereas $\Delta q_{\perp}^{\text{el}} \approx \text{const.}$ (i.e., a vertical line) in the large- Δk_{ph} region [$\Delta k_{\text{ph}} \gtrsim 1 \mu\text{m}^{-1}$; the hatched regime in Fig. 2(a)]. At the level of the expressions in Eqs. (15) and (16), this behavior can be understood as follows. From Eq. (16), when $\Delta k_{\text{ph}} \ll k_c$ and $\Delta k_{\text{ph}} \ll \Delta q_{\parallel}^{\text{el}}$, the dominant contribution to $\langle [\Delta(x_{\text{el}} - x_{\text{ph}})]^2 \rangle$ scales as $1/\Delta k_{\text{ph}}^2$ [the leading term in \mathcal{N}_g for $\Delta k_{\text{ph}} \ll k_c$ is proportional to $1/(k_c^2 \Delta k_{\text{ph}})$; see Eq. (10)]. Combining this with Eq. (15), we obtain $\mathcal{D}_{\text{sc}}^2 \propto (\Delta q_{\perp}^{\text{el}}/\Delta k_{\text{ph}})^2$ in this regime. This leads to $\Delta k_{\text{ph}} \propto \Delta q_{\perp}^{\text{el}}$ along the line $\mathcal{D}_{\text{sc}}^2 = 1$ for small Δk_{ph} . On the other hand, when $\Delta k_{\text{ph}} \gg \Delta q_{\parallel}^{\text{el}}$, the dominant contribution to $\langle [\Delta(x_{\text{el}} - x_{\text{ph}})]^2 \rangle$ scales as $1/(q_{\parallel}^{\text{el}})^2$. Combining this with Eq. (15), we obtain $\mathcal{D}_{\text{sc}}^2 \propto (\Delta q_{\perp}^{\text{el}}/q_{\parallel}^{\text{el}})^2$ in this regime. This implies $\Delta q_{\perp}^{\text{el}} \propto q_{\parallel}^{\text{el}}$ (independent of Δk_{ph}) along the line $\mathcal{D}_{\text{sc}}^2 = 1$ for large Δk_{ph} .

C. Wave-like, particle-like, and classical regimes

By comparing the results for \mathcal{P}_{sc} in Fig. 2(b) and $\mathcal{D}_{\text{sc}}^2$ in Fig. 2(c), we identify three distinct parameter regimes, labeled A, B, and C in Fig. 2(a). Regime A corresponds to strong entanglement according to both measures. Regime B exhibits strong entanglement in terms

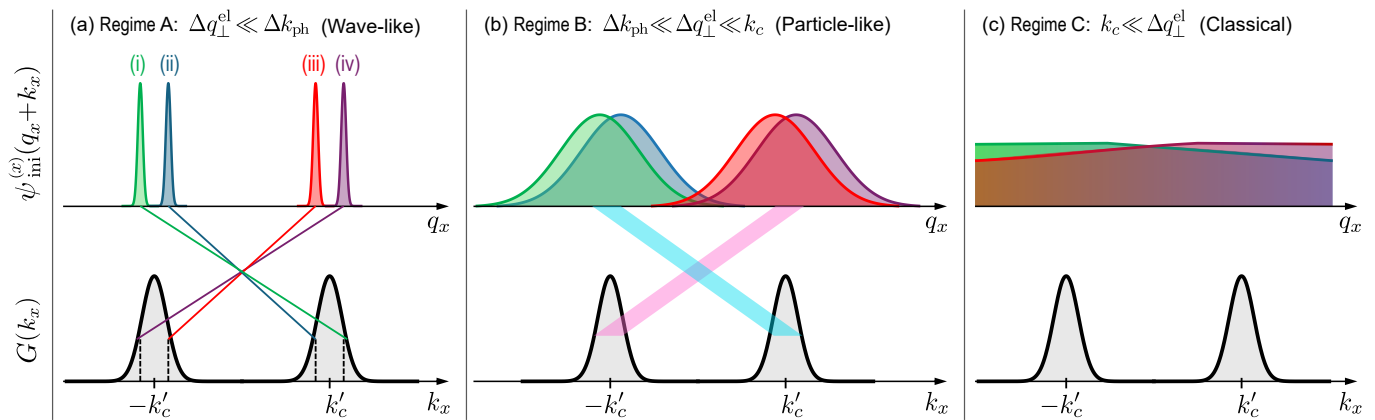


FIG. 3. Schematic illustrations of the x -directional wavevector-space functions in Eq. (17) shown for the three regimes labeled A, B, and C in Fig. 2(a). The upper panels depict $\psi_{\text{ini}}^{(x)}(q_x + k_x)$ for (i) $k_x = k'_c + \Delta k_{\text{ph}}$, (ii) $k_x = k'_c - \Delta k_{\text{ph}}$, (iii) $k_x = -k'_c + \Delta k_{\text{ph}}$, and (iv) $k_x = -k'_c - \Delta k_{\text{ph}}$. The lower panels depict $G(k_x)$. (a) Regime A, where $\Delta q_{\perp}^{\text{el}} \ll \Delta k_{\text{ph}}$. The functions $\psi_{\text{ini}}^{(x)}(q_x + k_x)$ of q_x for different k_x are distinguishable within each of the two peaks of $G(k_x)$, which leads to nearly one-to-one correlation (represented by thin lines): for each photon with k_x , a corresponding electron with $q_x = -k_x$ is correlated. (b) Regime B, where $\Delta k_{\text{ph}} \ll \Delta q_{\perp}^{\text{el}} \ll k_c$. The functions $\psi_{\text{ini}}^{(x)}(q_x + k_x)$ for different k_x are indistinguishable within each peak of $G(k_x)$ but distinguishable between the two peaks, which leads to less specific correlations (represented by thick lines): photons traveling in the positive direction tend to correlate with electrons traveling in the negative direction, and vice versa, but without a sharp one-to-one correspondence. (c) Regime C, where $k_c \ll \Delta q_{\perp}^{\text{el}}$. The functions $\psi_{\text{ini}}^{(x)}(q_x + k_x)$ for different k_x are indistinguishable even between the two peaks of $G(k_x)$. As explained in the main text, Regimes A, B, and C corresponds to the wave-like, particle-like, and classical regimes, respectively.

of \mathcal{P}_{sc} but not according to $\mathcal{D}_{\text{sc}}^2$. Regime C corresponds to almost separable (non-entangled) regime. As we will discuss in Sec. IV D, this parameter space is also divided into small- and large- Δk_{ph} regimes, which are distinguished by the hatching in Fig. 2(a). In this subsection, we focus on the unhatched (small- Δk_{ph}) regime in Fig. 2(a) and provide a qualitative understanding of Regimes A, B, and C. We show that these regimes can be identified with the wave-like, particle-like, and classical regimes. While the earlier work [21] formulated this classification in frequency (energy) space, we extend it here to wavevector (momentum) space and present the typical forms of the electron-photon state in each regime.

To this end, we note the following result from Eqs. (2), (3) and (7). For $\Delta k_{\text{ph}} \ll \Delta q_{\parallel}^{\text{el}}$, the width $\Delta q_{\parallel}^{\text{el}}$ of $\psi_{\text{ini}}^{(z)}(q_z + ck/v_z)$ in $|\Psi_{\text{sc}}\rangle$ is so broad that the electron's longitudinal (z -directional) degree of freedom is approximately separable from the remaining (electron's transverse and photonic) degrees of freedom. In this case, the scattered state in the x direction is roughly expressed as

$$|\Psi_{\text{sc},x}\rangle \approx \int dk_x dq_x G(k_x) \psi_{\text{ini}}^{(x)}(q_x + k_x) |q_x\rangle_{\text{el}} |k_x\rangle_{\text{ph}}, \quad (17)$$

where $|q_x\rangle_{\text{el}}$ ($|k_x\rangle_{\text{ph}}$) denotes the electron's (photon's) wavevector state in the x direction. The function $G(k_x)$ has two peaks located around $\pm k'_c$, where k'_c is of the same order of magnitude as k_c , each with a width of approximately Δk_{ph} . When $\Delta k_{\text{ph}} \ll k_c$, the two peaks are well separated, as illustrated in Fig. 3. Strictly speak-

ing, $|\Psi_{\text{sc}}\rangle$ cannot be reduced to $|\Psi_{\text{sc},x}\rangle$, since the electron's x -directional degree of freedom is entangled not only with the photonic x -directional degree of freedom but also with all photonic degrees of freedom and the electron's y -directional degree of freedom. Nevertheless, Eq. (17) is sufficient for the following qualitative discussion.

In Regime A, since $\Delta q_{\perp}^{\text{el}} \ll \Delta k_{\text{ph}}$, the Gaussian function $\psi_{\text{ini}}^{(x)}(q_x + k_x)$ can be approximated as a delta-like function within each of the two peaks of $G(k_x)$ in wavevector space, as schematically illustrated in Fig. 3(a). This sharp behavior in the wave-like regime was also discussed in frequency space [21]. As a result, Eq. (17) reduces to an EPR-like state,

$$|\Psi_{\text{sc},x}\rangle \approx \int dk_x G(k_x) | -k_x \rangle_{\text{el}} | k_x \rangle_{\text{ph}}.$$

Therefore, the entanglement is detected both by \mathcal{P}_{sc} and by $\mathcal{D}_{\text{sc}}^2$ in this regime. Moreover, if the photonic state is known to be $|k_x\rangle_{\text{ph}}$, the electron state is approximately a plane-wave state, $| -k_x \rangle_{\text{el}}$. In this sense, Regime A corresponds to the wave-like regime.

In Regime B, since $\Delta k_{\text{ph}} \ll \Delta q_{\perp}^{\text{el}} \ll k_c$, the variation of $\psi_{\text{ini}}^{(x)}(q_x + k_x)$ for different k_x cannot be resolved within each peak of $G(k_x)$ in wavevector space, as schematically illustrated in Fig. 3(b). This broad behavior in the particle-like regime was also discussed in frequency space [21]. Consequently, Eq. (17) can be further approximated

as

$$|\Psi_{\text{sc},x}\rangle \approx \int dq_x \psi_{\text{ini}}^{(x)}(q_x + k_c) |q_x\rangle_{\text{el}} \int_0^\infty dk_x G(k_x) |k_x\rangle_{\text{ph}} \\ + \int dq_x \psi_{\text{ini}}^{(x)}(q_x - k_c) |q_x\rangle_{\text{el}} \int_{-\infty}^0 dk_x G(k_x) |k_x\rangle_{\text{ph}}.$$

This represents a superposition of two distinct states. We note that in the full two-dimensional transverse space, the electron and photon are also entangled in the direction of azimuthal angle ϕ . Since the angle ϕ is a continuous variable, there remain nearly infinitely many Schmidt modes, and therefore $\mathcal{P}_{\text{sc}} \simeq 0$, even though $\mathcal{D}_{\text{sc}}^2$ does not detect entanglement in this regime. Moreover, if the photonic state is known to be $|k_x\rangle_{\text{ph}}$, the electron state becomes a wave-packet (particle-like) state approximately given by $\int dq_x \psi_{\text{ini}}^{(x)}(q_x + \text{sgn}(k_x)k_c) |q_x\rangle_{\text{el}}$. In this sense, Regime B corresponds to the particle-like regime.

In Regime C, where $k_c \ll \Delta q_{\perp}^{\text{el}}$, the function $\psi_{\text{ini}}^{(x)}(q_x + k_x)$ for different k_x cannot be resolved even between $k_x = k_c$ and $k_x = -k_c$, as schematically illustrated in Fig. 3(c). Accordingly, Eq. (17) reduces to

$$|\Psi_{\text{sc},x}\rangle \approx \int dq_x \psi_{\text{ini}}^{(x)}(q_x) |q_x\rangle_{\text{el}} \int dk_x G(k_x) |k_x\rangle_{\text{ph}}.$$

This is a separable state, leading to $\mathcal{P}_{\text{sc}} \simeq 1$ and $\mathcal{D}_{\text{sc}}^2 \geq 1$. Therefore, this regime corresponds to the classical regime.

In summary, in the small- Δk_{ph} regime ($\Delta k_{\text{ph}} \ll \Delta q_{\parallel}^{\text{el}}$ and $\Delta k_{\text{ph}} \ll k_c$), the boundary between Regimes A and B lies around $\Delta q_{\perp}^{\text{el}} \approx \Delta k_{\text{ph}}$, while that between Regimes B and C lies around $\Delta q_{\perp}^{\text{el}} \approx k_c$.

D. Influence of electron longitudinal coherence

We next examine how the longitudinal coherence of the electron beam affects the entanglement. Figures 4(a) and (c) show the subsystem purity \mathcal{P}_{sc} for different values of $L_{\parallel}^{\text{el}}$. Compared with Fig. 2(b), as $L_{\parallel}^{\text{el}}$ increases ($\Delta q_{\parallel}^{\text{el}}$ decreases), the region where \mathcal{P}_{sc} indicates strong entanglement expands toward Regime C [upper right of Fig. 4(c)]. Figures 4(b) and (d) show the corresponding uncertainty product $\mathcal{D}_{\text{sc}}^2$. Compared with Fig. 2(c), as $L_{\parallel}^{\text{el}}$ increases ($\Delta q_{\parallel}^{\text{el}}$ decreases), the region where $\mathcal{D}_{\text{sc}}^2$ fails to detect entanglement grows toward Regime A. This behavior can be understood, at the level of Eq. (16), as arising from the term $c^2/[14v_z^2(\Delta q_{\parallel}^{\text{el}})^2]$.

The origin of these seemingly opposite trends of \mathcal{P}_{sc} and $\mathcal{D}_{\text{sc}}^2$ can be explained as follows. As $L_{\parallel}^{\text{el}}$ increases, the width $\Delta q_{\parallel}^{\text{el}}$ of $\psi_{\text{ini}}^{(z)}(q_z + ck/v_z)$ in $|\Psi_{\text{sc}}\rangle$ [Eq. (2) with Eq. (3)] becomes narrower. When $\Delta q_{\parallel}^{\text{el}} < \Delta k_{\text{ph}}$, the entanglement between the electron's longitudinal (z -directional) degree of freedom and the photonic degrees of freedom becomes significant in a manner similar to

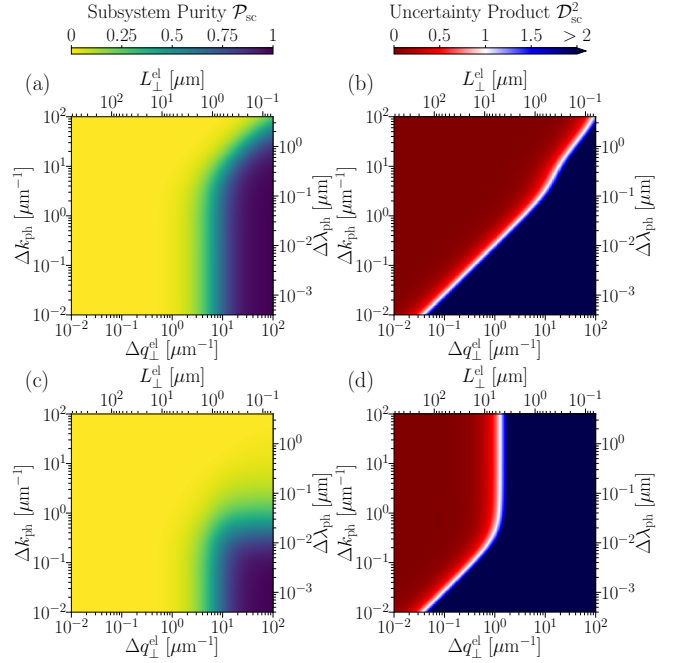


FIG. 4. Entanglement measures of the scattered state $|\Psi_{\text{sc}}\rangle$ for different values of $L_{\parallel}^{\text{el}}$, plotted as functions of $\Delta q_{\perp}^{\text{el}}$ and Δk_{ph} . Left panels [(a) and (c)] show the results for the subsystem purity \mathcal{P}_{sc} , and right panels [(b) and (d)] show those for the uncertainty product $\mathcal{D}_{\text{sc}}^2$. (a) and (b): Results for $L_{\parallel}^{\text{el}} = 0.13 \mu\text{m}$ ($\Delta q_{\parallel}^{\text{el}} \simeq 48.3 \mu\text{m}^{-1}$). (c) and (d): Results for $L_{\parallel}^{\text{el}} = 13 \mu\text{m}$ ($\Delta q_{\parallel}^{\text{el}} \simeq 0.483 \mu\text{m}^{-1}$). The other parameter values are the same as those in Fig. 2.

that discussed in Sec. IV C. Consequently, the electron-photon entanglement detected by \mathcal{P}_{sc} is present in the region $\Delta k_{\text{ph}} > \Delta q_{\parallel}^{\text{el}}$, and the region extends as $L_{\parallel}^{\text{el}}$ increases [Figs. 2(b) and 4(c)].

Since the argument of $\psi_{\text{ini}}^{(z)}(q_z + ck/v_z)$ depends on q_z and k_{\perp} , the electron's longitudinal degree of freedom becomes entangled with the photonic transverse degrees of freedom for $\Delta k_{\text{ph}} > \Delta q_{\parallel}^{\text{el}}$. Moreover, when $\Delta q_{\parallel}^{\text{el}} < \Delta q_{\perp}^{\text{el}}$ in addition to $\Delta q_{\parallel}^{\text{el}} < \Delta k_{\text{ph}}$, the width of $\psi_{\text{ini}}^{(z)}(q_z + ck/v_z)$ becomes smaller than that of $\psi_{\text{ini}}^{(x)}(q_x + k_x)$. As a result, the quantum correlation involving the electron's longitudinal degree of freedom becomes stronger than that involving the electron's transverse degrees of freedom. Consequently, the transverse EPR correlation between the electron's and photon's x -degrees of freedom leaks into correlations involving the electron's z -degree of freedom. This weakens the transverse EPR correlation, causing $\mathcal{D}_{\text{sc}}^2$ to fail to detect entanglement. Indeed, in the upper region ($\Delta k_{\text{ph}} > \Delta q_{\parallel}^{\text{el}}$) in Figs. 2(c) and 4(d), $\mathcal{D}_{\text{sc}}^2 > 1$ for $\Delta q_{\perp}^{\text{el}} \gtrsim 2\Delta q_{\parallel}^{\text{el}}$.

To confirm the behavior of the entanglement involving the electron's longitudinal degree of freedom in the above discussion, we examine the subsystem purity $\mathcal{P}_z^{\text{el}}$ of the

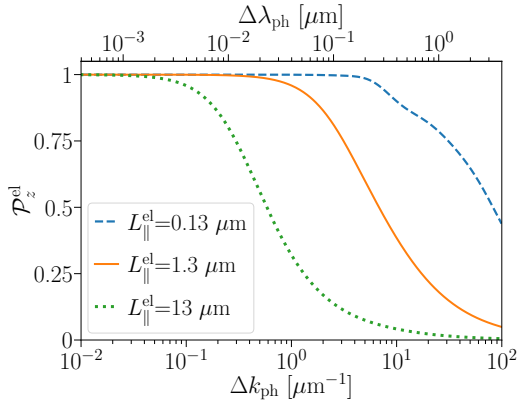


FIG. 5. Subsystem purity $\mathcal{P}_z^{\text{el}}$ of the electron's z -degree of freedom in the scattered state $|\Psi_{\text{sc}}\rangle$ as a function of the luminescence spectral width Δk_{ph} . The dashed, solid, and dotted curves correspond to $L_{\parallel}^{\text{el}} = 0.13, 1.3$ and $13 \mu\text{m}$ ($\Delta q_{\parallel}^{\text{el}} \simeq 48.3, 4.83$ and $0.483 \mu\text{m}^{-1}$), respectively. The other parameter values are the same as those in Fig. 2.

electron's z -degree of freedom. $\mathcal{P}_z^{\text{el}}$ is defined as

$$\mathcal{P}_z^{\text{el}} = \text{Tr}_z^{\text{el}} \left[\left(\text{Tr}_{xy}^{\text{el}} \text{Tr}_{\text{ph}} |\Psi_{\text{sc}}\rangle \langle \Psi_{\text{sc}}| \right)^2 \right], \quad (18)$$

where Tr_z^{el} and $\text{Tr}_{xy}^{\text{el}}$ denote the traces over the electron's z and xy degrees of freedom, respectively. Similarly to \mathcal{P}_{sc} , $\mathcal{P}_z^{\text{el}}$ satisfies $0 \leq \mathcal{P}_z^{\text{el}} \leq 1$, and a small value of $\mathcal{P}_z^{\text{el}}$ indicates significant entanglement involving the electron's longitudinal degree of freedom. Using Eqs. (2) and (3) for $|\Psi_{\text{sc}}\rangle$ with Eqs. (5) and (6) for ψ_{ini} in a manner similar to that in Eq. (12), we obtain

$$\mathcal{P}_z^{\text{el}} = \int d^3k d^3k' \Gamma(\mathbf{k}) \Gamma(\mathbf{k}') \exp \left[-\frac{c^2(k-k')^2}{4v_z^2(\Delta q_{\parallel}^{\text{el}})^2} \right]. \quad (19)$$

We note that this is independent of both $\Delta q_{\perp}^{\text{el}}$ and $\eta(\mathbf{k})$.

Figure 5 shows the numerical results of $\mathcal{P}_z^{\text{el}}$ for several values of $L_{\parallel}^{\text{el}}$, plotted against Δk_{ph} . We find that $\mathcal{P}_z^{\text{el}}$ starts to decrease from unity around $\Delta k_{\text{ph}} \approx \Delta q_{\parallel}^{\text{el}}$. This confirms that the electron's longitudinal degree of freedom becomes significantly entangled with the remaining ones for $\Delta k_{\text{ph}} > \Delta q_{\parallel}^{\text{el}}$. In Fig. 2(a), to explicitly indicate the region where this type of entanglement is present, we apply hatching to the area with $\mathcal{P}_z^{\text{el}} < 2/3$.

Finally in this subsection, we discuss the upper region ($\Delta k_{\text{ph}} \gtrsim 10 \mu\text{m}^{-1}$) in Figs. 4(a) and (b), where we observe that $\Delta q_{\perp}^{\text{el}} \propto \Delta k_{\text{ph}}$ along the boundaries in both plots. In these plots, since $\Delta k_{\text{ph}} < \Delta q_{\parallel}^{\text{el}}$, the electron's longitudinal degree of freedom is approximately separable from the remaining ones. Therefore, Eq. (17) is applicable. However, since $\Delta k_{\text{ph}} > k_c$ also holds in the upper region, the two peaks of $G(k_x)$ in Eq. (17) merge into a single peak with a width Δk_{ph} . Consequently, the particle-like regime [corresponding to Fig. 3(b)] is absent in this situation, and the boundary between the entangled and classical regimes satisfies $\Delta q_{\perp}^{\text{el}} \approx \Delta k_{\text{ph}}$.

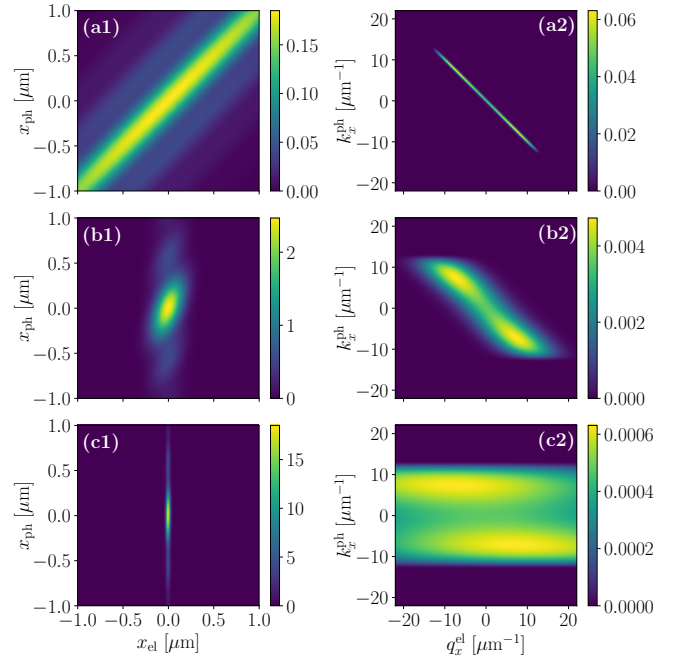


FIG. 6. The electron–photon joint probability distributions along the x direction for the states indicated by the cross symbols for $\Delta k_{\text{ph}} = 0.3 \mu\text{m}^{-1}$ ($\Delta \lambda_{\text{ph}} \simeq 0.119 \mu\text{m}$) in Fig. 2(a). The left panels show the spatial distributions $P(x_{\text{el}}, x_{\text{ph}})$, and the right panels show the wavevector distributions $P(q_x^{\text{el}}, k_x^{\text{ph}})$. (a1) and (a2) correspond to $L_{\perp}^{\text{el}} = 20 \mu\text{m}$ ($\Delta q_{\perp}^{\text{el}} \simeq 0.314 \mu\text{m}^{-1}$), (b1) and (b2) to $L_{\perp}^{\text{el}} = 1.5 \mu\text{m}$ ($\Delta q_{\perp}^{\text{el}} \simeq 4.19 \mu\text{m}^{-1}$), and (c1) and (c2) to $L_{\perp}^{\text{el}} = 0.2 \mu\text{m}$ ($\Delta q_{\perp}^{\text{el}} \simeq 31.4 \mu\text{m}^{-1}$). The other parameter values are the same as those in Fig. 2.

E. Electron–photon joint probability distribution

Finally, we examine the electron–photon joint probability distributions in the scattered state $|\Psi_{\text{sc}}\rangle$ in the three regimes. The distributions can be measured by coincidence counts in experiments. Using Eqs. (2) and (3) for $|\Psi_{\text{sc}}\rangle$ and with Eqs. (5) and (6) for ψ_{ini} , we find that the joint spatial distribution in the x direction is given by

$$P(x_{\text{el}}, x_{\text{ph}}) = \frac{1}{\sqrt{2\pi^3}} \Delta q_{\perp}^{\text{el}} e^{-2(\Delta q_{\perp}^{\text{el}})^2 x_{\text{el}}^2} \times \int dk_x dk_y dk_z dk'_x \sqrt{\Gamma(\mathbf{k}) \Gamma(\mathbf{k}')} e^{i[\eta(\mathbf{k}) - \eta(\mathbf{k}')] - i(k_x - k'_x)(x_{\text{el}} - x_{\text{ph}}) - c^2(k - k')^2 / [8v_z^2(\Delta q_{\parallel}^{\text{el}})^2]}, \quad (20)$$

where $\mathbf{k} = (k_x, k_y, k_z)$, $\mathbf{k}' = (k'_x, k_y, k_z)$, $k = |\mathbf{k}|$, and $k' = |\mathbf{k}'|$ (see Appendix C1 for the derivation of this equation). We also find that the joint wavevector (momentum) distribution in the x direction is given by

$$P(q_x^{\text{el}}, k_x^{\text{ph}}) = |\psi_{\text{ini}}^{(x)}(q_x^{\text{el}} + k_x^{\text{ph}})|^2 \int dk_y^{\text{ph}} dk_z^{\text{ph}} \Gamma(\mathbf{k}^{\text{ph}}), \quad (21)$$

where $\mathbf{k}^{\text{ph}} = (k_x^{\text{ph}}, k_y^{\text{ph}}, k_z^{\text{ph}})$ (see Appendix C2 for the derivation of this equation). We note that $P(q_x^{\text{el}}, k_x^{\text{ph}})$ is independent of the undetermined phase $\eta(\mathbf{k})$.

We evaluate these distributions by substituting the model for $\Gamma(\mathbf{k})$ [Eqs. (7)–(9)] into the above expressions and numerically computing the integrals. For the evaluation of $P(x_{\text{el}}, x_{\text{ph}})$, we neglect the phase factor $e^{i[\eta(\mathbf{k}) - \eta(\mathbf{k}')]}$ in Eq. (20), assuming that the phase in $|\Psi_{\text{sc}}\rangle$ is eliminated by a local operation on the photon.

Figure 6 shows the results: the left panels display the spatial distributions and the right panels display the wavevector distributions. In Regime A (wave-like regime), both the spatial and wavevector distributions exhibit strong correlations, as seen in Figs. 6(a1) and 6(a2). In Regime B (particle-like regime), the spatial correlations are largely washed out, as seen in Fig. 6(b1), whereas the wavevector distribution retains a characteristic bimodal structure corresponding to $k_x \simeq \pm k_c$, as shown in Fig. 6(b2). This structure reflects the two-component entangled state discussed in Sec. IV C. In Regime C (classical regime), both the spatial and wavevector joint distributions exhibit no noticeable correlations, as shown in Figs. 6(c1) and 6(c2). This confirms that the scattered state has almost no entanglement in this regime.

V. CONCLUSION

We have developed a theoretical framework to describe the quantum state of electron–photon pairs generated in coherent cathodoluminescence (CL), in which the scattered state $|\Psi_{\text{sc}}\rangle$ is reconstructed from the experimentally accessible luminescence spectrum. Within this framework, we have quantified the entanglement of the scattered state using the subsystem purities \mathcal{P}_{sc} and $\mathcal{P}_z^{\text{el}}$, together with the EPR-type uncertainty product $\mathcal{D}_{\text{sc}}^2$. These measures reveal three distinct regimes—wave-like, particle-like, and classical—each characterized by qualitatively different structures of transverse quantum correlations. We have shown that these regimes are governed by the interplay between the transverse and longitudinal coherence of the electron beam and the spectral width of the emitted photons. Our analysis further demonstrates that increasing the longitudinal coherence of the electron beam induces additional correlations involving the longitudinal degree of freedom, which in turn degrade the transverse EPR correlations. This result indicates that a relatively short longitudinal coherence is favorable for generating strongly entangled electron–photon pairs with pronounced transverse quantum correlations.

The framework assumes translational invariance in the transverse plane (perpendicular to the electron beam) and is applicable to transition radiation, a typical coherent CL process. Extending it to cases where this assumption does not hold—such as Cherenkov radiation and Smith-Purcell effect—remains a subject for future work.

Our findings provide a unified perspective on quantum correlations in CL and offer practical guidelines for engineering entangled electron–photon states. This opens new possibilities for applications such as quantum imaging, quantum sensing, and other emerging quantum-enabled techniques in electron microscopy.

ACKNOWLEDGMENTS

This work was supported by JST CREST Grant No. JPMJCR2513 and JSPS KAKENHI Grants No. JP18K03454, No. JP21K18195, No. JP22H01963, No. JP23K23231, and No. JP22H05032. One of the authors (K.A.) is grateful to Dr. Takeshi Ohshima for his valuable support for the research.

Appendix A: Derivation of the scattered state

In this appendix, we derive the scattered state $|\Psi_{\text{sc}}\rangle$ in Eq. (2) with Eq. (3). In the derivation, we use a perturbation theory in the electron–photon interaction \hat{H}_{int} and the in-plane momentum conservation condition [Eq. (1)] for \hat{H}_{int} .

1. Perturbation theory

In this paper, we consider the case in which each electron in the electron beam induces at most one photon emission, if it occurs. In general, a state of the electron–photon system whose photon number is zero or one is expressed as

$$|\Psi(t)\rangle = \int d^3q \alpha_0(t, \mathbf{q}) e^{-i\varepsilon_{\mathbf{q}}t} |\mathbf{q}, \text{vac}\rangle + \int d^3q d^3k \alpha_1(t, \mathbf{q}, \mathbf{k}) e^{-i(\varepsilon_{\mathbf{q}} + \omega_{\mathbf{k}})t} |\mathbf{q}, \mathbf{k}\rangle, \quad (\text{A1})$$

where $\varepsilon_{\mathbf{q}} = \hbar q^2 / (2m)$ and $\omega_{\mathbf{k}} = ck$. Since the initial state is $|\Psi_{\text{ini}}\rangle = \int d^3q \psi_{\text{ini}}(\mathbf{q}) |\mathbf{q}, \text{vac}\rangle$, the initial condition for the amplitudes $\alpha_0(t, \mathbf{q})$ and $\alpha_1(t, \mathbf{q}, \mathbf{k})$ are given by

$$\alpha_{0, \text{ini}}(\mathbf{q}) = \psi_{\text{ini}}(\mathbf{q}), \quad (\text{A2})$$

$$\alpha_{1, \text{ini}}(\mathbf{q}, \mathbf{k}) = 0. \quad (\text{A3})$$

By inserting the expression (A1) into the Schrödinger equation $i\hbar \frac{\partial}{\partial t} |\Psi(t)\rangle = \hat{H} |\Psi(t)\rangle$, we obtain

$$\frac{\partial}{\partial t} \alpha_0(t, \mathbf{q}) = -\frac{i}{\hbar} \int d^3q' d^3k' e^{i(\varepsilon_{\mathbf{q}} - \varepsilon_{\mathbf{q}'} - \omega_{\mathbf{k}'})t} \times \langle \mathbf{q}, \text{vac} | \hat{H}_{\text{int}} | \mathbf{q}', \mathbf{k}' \rangle \alpha_1(t, \mathbf{q}', \mathbf{k}'), \quad (\text{A4})$$

$$\frac{\partial}{\partial t} \alpha_1(t, \mathbf{q}, \mathbf{k}) = -\frac{i}{\hbar} \int d^3q' e^{i(\varepsilon_{\mathbf{q}} - \varepsilon_{\mathbf{q}'} + \omega_{\mathbf{k}})t} \times \langle \mathbf{q}, \mathbf{k} | \hat{H}_{\text{int}} | \mathbf{q}', \text{vac} \rangle \alpha_0(t, \mathbf{q}'). \quad (\text{A5})$$

We expand the amplitudes up to the second order in \hat{H}_{int} : $\alpha_0(t, \mathbf{q}) = \alpha_0^{(0)}(t, \mathbf{q}) + \alpha_0^{(1)}(t, \mathbf{q}) + \alpha_0^{(2)}(t, \mathbf{q})$ and $\alpha_1(t, \mathbf{q}, \mathbf{k}) = \alpha_1^{(0)}(t, \mathbf{q}, \mathbf{k}) + \alpha_1^{(1)}(t, \mathbf{q}, \mathbf{k}) + \alpha_1^{(2)}(t, \mathbf{q}, \mathbf{k})$, where $\alpha_0^{(j)}$ and $\alpha_1^{(j)}$ are the j -th-order amplitudes. The zeroth-order equations for Eqs. (A4) and (A5) are respectively given by

$$\frac{\partial}{\partial t} \alpha_0^{(0)}(t, \mathbf{q}) = 0, \quad (\text{A6})$$

$$\frac{\partial}{\partial t} \alpha_1^{(0)}(t, \mathbf{q}, \mathbf{k}) = 0. \quad (\text{A7})$$

Therefore the initial conditions (A2) and (A3) yield

$$\alpha_0^{(0)}(t, \mathbf{q}) = \psi_{\text{ini}}(\mathbf{q}), \quad (\text{A8})$$

$$\alpha_1^{(0)}(t, \mathbf{q}, \mathbf{k}) = 0. \quad (\text{A9})$$

With these zeroth-order solutions, the first-order equations for Eqs. (A4) and (A5) are respectively given by

$$\frac{\partial}{\partial t} \alpha_0^{(1)}(t, \mathbf{q}) = 0, \quad (\text{A10})$$

$$\begin{aligned} \frac{\partial}{\partial t} \alpha_1^{(1)}(t, \mathbf{q}, \mathbf{k}) &= -\frac{i}{\hbar} \int d^3 q' e^{i(\varepsilon_{\mathbf{q}} - \varepsilon_{\mathbf{q}'} + \omega_{\mathbf{k}})t} \\ &\times \langle \mathbf{q}, \mathbf{k} | \hat{H}_{\text{int}} | \mathbf{q}', \text{vac} \rangle \psi_{\text{ini}}(\mathbf{q}'). \end{aligned} \quad (\text{A11})$$

From Eq. (A10), we have

$$\alpha_0^{(1)}(t, \mathbf{q}) = 0. \quad (\text{A12})$$

We integrate Eq. (A11) in time to obtain the amplitude after sufficiently long time as

$$\begin{aligned} \alpha_{1, \text{fin}}^{(1)}(\mathbf{q}, \mathbf{k}) &= -\frac{2\pi i}{\hbar} \int d^3 q' \delta(\varepsilon_{\mathbf{q}} - \varepsilon_{\mathbf{q}'} + \omega_{\mathbf{k}}) \\ &\times \langle \mathbf{q}, \mathbf{k} | \hat{H}_{\text{int}} | \mathbf{q}', \text{vac} \rangle \psi_{\text{ini}}(\mathbf{q}'). \end{aligned} \quad (\text{A13})$$

With Eq. (A12), the second-order equations for Eqs. (A4) and (A5) are respectively given by

$$\begin{aligned} \frac{\partial}{\partial t} \alpha_0^{(2)}(t, \mathbf{q}) &= -\frac{i}{\hbar} \int d^3 q' d^3 k' e^{i(\varepsilon_{\mathbf{q}} - \varepsilon_{\mathbf{q}'} - \omega_{\mathbf{k}'})t} \\ &\times \langle \mathbf{q}, \text{vac} | \hat{H}_{\text{int}} | \mathbf{q}', \mathbf{k}' \rangle \alpha_1^{(1)}(t, \mathbf{q}', \mathbf{k}'), \end{aligned} \quad (\text{A14})$$

$$\frac{\partial}{\partial t} \alpha_1^{(2)}(t, \mathbf{q}, \mathbf{k}) = 0. \quad (\text{A15})$$

From the latter we have

$$\alpha_1^{(2)}(t, \mathbf{q}, \mathbf{k}) = 0. \quad (\text{A16})$$

Putting Eqs. (A8), (A9), (A12), (A13) and (A16) together, we obtain the state after the scattering as

$$\begin{aligned} |\Psi'_{\text{fin}}\rangle &\propto \int d^3 q [\psi_{\text{ini}}(\mathbf{q}) + \alpha_{0, \text{fin}}^{(2)}(\mathbf{q})] e^{-i\varepsilon_{\mathbf{q}} t} |\mathbf{q}, \text{vac}\rangle \\ &+ \int d^3 q d^3 k \alpha_{1, \text{fin}}^{(1)}(\mathbf{q}, \mathbf{k}) e^{-i(\varepsilon_{\mathbf{q}} + \omega_{\mathbf{k}})t} |\mathbf{q}, \mathbf{k}\rangle, \end{aligned} \quad (\text{A17})$$

where $\alpha_{0, \text{fin}}^{(2)}(\mathbf{q})$ is the long-time solution of Eq. (A14). The phase factors $e^{-i\varepsilon_{\mathbf{q}} t}$ and $e^{-i(\varepsilon_{\mathbf{q}} + \omega_{\mathbf{k}})t}$ associated with the free propagation cancel out at the image plane when a lens system is employed. Furthermore, by taking the normalization of the state into consideration, we arrive at

$$|\Psi_{\text{fin}}\rangle = \sqrt{1-a} |\Psi_0\rangle + \sqrt{a} |\Psi_{\text{sc}}\rangle \quad (\text{A18})$$

with $a = A_1/(A_0 + A_1)$, where

$$A_0 = \int d^3 q |\psi_{\text{ini}}(\mathbf{q}) + \alpha_{0, \text{fin}}^{(2)}(\mathbf{q})|^2, \quad (\text{A19})$$

$$A_1 = \int d^3 q d^3 k |\alpha_{1, \text{fin}}^{(1)}(\mathbf{q}, \mathbf{k})|^2, \quad (\text{A20})$$

and

$$|\Psi_0\rangle = \int d^3 q \psi_0(\mathbf{q}) |\mathbf{q}, \text{vac}\rangle, \quad (\text{A21})$$

$$\psi_0(\mathbf{q}) = \frac{1}{\sqrt{A_0}} [\psi_{\text{ini}}(\mathbf{q}) + \alpha_{0, \text{fin}}^{(2)}(\mathbf{q})], \quad (\text{A22})$$

and

$$|\Psi_{\text{sc}}\rangle = \int d^3 q d^3 k \psi_{\text{sc}}(\mathbf{q}, \mathbf{k}) |\mathbf{q}, \mathbf{k}\rangle, \quad (\text{A23})$$

$$\psi_{\text{sc}}(\mathbf{q}, \mathbf{k}) = \frac{1}{\sqrt{A_1}} \alpha_{1, \text{fin}}^{(1)}(\mathbf{q}, \mathbf{k}). \quad (\text{A24})$$

2. Connection between the scattered state and the luminescence spectrum

To obtain the expression (3) of the scattered-state amplitude $\psi_{\text{sc}}(\mathbf{q}, \mathbf{k})$, we consider the excitation probability (luminescence spectrum) $\Gamma(\mathbf{k}) = \int d^3 q |\langle \mathbf{q}, \mathbf{k} | \Psi_{\text{sc}} \rangle|^2$ of a photon with a wavevector \mathbf{k} associated to this scattering event. From Eqs. (A23) and (A24), it is given by

$$\Gamma(\mathbf{k}) = \int d^3 q |\psi_{\text{sc}}(\mathbf{q}, \mathbf{k})|^2 = \frac{1}{A_1} \int d^3 q |\alpha_{1, \text{fin}}^{(1)}(\mathbf{q}, \mathbf{k})|^2. \quad (\text{A25})$$

To evaluate the right-hand side, we rewrite $\alpha_{1, \text{fin}}^{(1)}(\mathbf{q}, \mathbf{k})$ in Eq. (A13). As usual in coherent CL, we assume that the momentum change of the electron is sufficiently smaller than the mean momentum $\hbar q_0$ of an incident electron. We can thus approximate $\varepsilon_{\mathbf{q}} - \varepsilon_{\mathbf{q}'} \simeq \frac{\partial \varepsilon_{\mathbf{q}}}{\partial \mathbf{q}} \cdot (\mathbf{q} - \mathbf{q}') \simeq v_z(q_z - q'_z)$ with $v_z = \hbar q_0/m$. This approximation yields

$$\begin{aligned} \alpha_{1, \text{fin}}^{(1)}(\mathbf{q}, \mathbf{k}) &\simeq -\frac{2\pi i}{\hbar v_z} \int d^3 q' \delta(q_z - q'_z + ck/v_z) \\ &\times \langle \mathbf{q}, \mathbf{k} | \hat{H}_{\text{int}} | \mathbf{q}', \text{vac} \rangle \psi_{\text{ini}}(\mathbf{q}'). \end{aligned} \quad (\text{A26})$$

Furthermore, by using the in-plane momentum-conservation condition given in Eq. (1), we obtain

$$\alpha_{1, \text{fin}}^{(1)}(\mathbf{q}, \mathbf{k}) = -\frac{i}{(2\pi)^2} \psi_{\text{ini}}(\mathbf{q}_{\perp} + \mathbf{k}_{\perp}, q_z + ck/v_z) \tilde{\beta}(\mathbf{k}), \quad (\text{A27})$$

where $\tilde{\beta}(\mathbf{k}) = (1/v_z)(2\pi)^3 h(\mathbf{k}, -ck/v_z)$ is a function that depends only on \mathbf{k} .

By substituting Eq. (A27) into Eq. (A25) and using the normalization condition for $\psi_{\text{ini}}(\mathbf{q})$, we have

$$\begin{aligned}\Gamma(\mathbf{k}) &= \frac{1}{(2\pi)^4 A_1} \int d^3 q |\psi_{\text{ini}}(\mathbf{q}_\perp + \mathbf{k}_\perp, q_z + ck/v_z)|^2 |\tilde{\beta}(\mathbf{k})|^2 \\ &= \frac{1}{(2\pi)^4 A_1} |\tilde{\beta}(\mathbf{k})|^2.\end{aligned}\quad (\text{A28})$$

By inverting this relation, we obtain $\tilde{\beta}(\mathbf{k}) =$

$i(2\pi)^2 \sqrt{A_1 \Gamma(\mathbf{k})} e^{i\eta(\mathbf{k})}$, where $\eta(\mathbf{k})$ is a phase that cannot be inferred from the luminescence spectrum $\Gamma(\mathbf{k})$ alone and may depend on \mathbf{k} . From this relation and Eqs. (A24) and (A27), we arrive at the desired expression (3) for $\psi_{\text{sc}}(\mathbf{q}, \mathbf{k})$. Since the luminescence spectrum $\Gamma(\mathbf{k})$ is experimentally accessible, this relation enables us to reconstruct the scattered state $|\Psi_{\text{sc}}\rangle$ of the electron-photon system from experimental data, up to the undetermined phase $\eta(\mathbf{k})$. We note that since $\tilde{\beta}(\mathbf{k}) = (1/v_z)(2\pi)^3 h(\mathbf{k}, -ck/v_z)$ and $h(\mathbf{k}, -ck/v_z)$ is invariant under rotations in the transverse plane (i.e., independent of the azimuthal angle ϕ), $\Gamma(\mathbf{k})$ and $\eta(\mathbf{k})$ also inherit the same rotational symmetry.

Appendix B: Calculation of the subsystem purity

In this appendix, we calculate the subsystem purity $\mathcal{P}_{\text{sc}} = \text{Tr}_{\text{el}}[(\text{Tr}_{\text{ph}} |\Psi_{\text{sc}}\rangle\langle\Psi_{\text{sc}}|)^2]$ of the scattered state to derive Eq. (12).

The electron's reduced density matrix for the scattered state $|\Psi_{\text{sc}}\rangle$ is given by

$$\begin{aligned}\hat{\rho}_{\text{el}} &= \text{Tr}_{\text{ph}} |\Psi_{\text{sc}}\rangle\langle\Psi_{\text{sc}}| \\ &= \int d^3 k \langle \mathbf{k} |_{\text{ph}} (|\Psi_{\text{sc}}\rangle\langle\Psi_{\text{sc}}|) | \mathbf{k} \rangle_{\text{ph}} \\ &= \int d^3 q d^3 q' d^3 k \psi_{\text{sc}}^*(\mathbf{q}', \mathbf{k}) \psi_{\text{sc}}(\mathbf{q}, \mathbf{k}) | \mathbf{q} \rangle_{\text{el}} \langle \mathbf{q}' |_{\text{el}}.\end{aligned}$$

We then calculate \mathcal{P}_{sc} as

$$\begin{aligned}\mathcal{P}_{\text{sc}} &= \text{Tr}_{\text{el}}[\hat{\rho}_{\text{el}}^2] \\ &= \int d^3 q \langle \mathbf{q} |_{\text{el}} \hat{\rho}_{\text{el}}^2 | \mathbf{q} \rangle_{\text{el}} \\ &= \int d^3 q d^3 q' d^3 k d^3 k' \psi_{\text{sc}}^*(\mathbf{q}', \mathbf{k}) \psi_{\text{sc}}(\mathbf{q}, \mathbf{k}) \psi_{\text{sc}}^*(\mathbf{q}', \mathbf{k}') \psi_{\text{sc}}(\mathbf{q}, \mathbf{k}') \\ &= \int d^3 k d^3 k' \Gamma(\mathbf{k}) \Gamma(\mathbf{k}') \left[\int d^3 q \psi_{\text{ini}}(\mathbf{q}_\perp + \mathbf{k}_\perp, q_z + \frac{ck}{v_z}) \psi_{\text{ini}}(\mathbf{q}_\perp + \mathbf{k}'_\perp, q_z + \frac{ck'}{v_z}) \right]^2.\end{aligned}\quad (\text{B1})$$

We have used the fact that $\psi_{\text{ini}}(\mathbf{q})$ is a real-valued function. Using Eqs. (5) and (6) for $\psi_{\text{ini}}(\mathbf{q})$, we can calculate the integral in the square bracket of the above equation as

$$\int d^3 q \psi_{\text{ini}}(\mathbf{q}_\perp + \mathbf{k}_\perp, q_z + ck/v_z) \psi_{\text{ini}}(\mathbf{q}_\perp + \mathbf{k}'_\perp, q_z + ck'/v_z) = \exp\left[-\frac{|\mathbf{k}_\perp - \mathbf{k}'_\perp|^2}{8(\Delta q_\perp^{\text{el}})^2} - \frac{c^2(k - k')^2}{8v_z^2(\Delta q_\parallel^{\text{el}})^2}\right].\quad (\text{B2})$$

Substituting this result into Eq. (B1), we obtain Eq. (12).

Appendix C: Calculation of the joint probability distributions

1. Joint spatial distribution $P(x_{\text{el}}, x_{\text{ph}})$

We here derive Eq. (20) for the joint probability distribution $P(x_{\text{el}}, x_{\text{ph}})$ that the electron is at x_{el} and the photon is at x_{ph} in the x direction.

The joint distribution $P(x_{\text{el}}, x_{\text{ph}})$ is defined by

$$P(x_{\text{el}}, x_{\text{ph}}) = \int dy_{\text{el}} dz_{\text{el}} dy_{\text{ph}} dz_{\text{ph}} |\langle \mathbf{r}_{\text{el}}, \mathbf{r}_{\text{ph}} | \Psi_{\text{sc}} \rangle|^2, \quad (\text{C1})$$

where $\mathbf{r}_{\text{el}} = (x_{\text{el}}, y_{\text{el}}, z_{\text{el}})$ and $\mathbf{r}_{\text{ph}} = (x_{\text{ph}}, y_{\text{ph}}, z_{\text{ph}})$.

Using Eqs. (2) and (3) and $\langle \mathbf{r}_{\text{el}}, \mathbf{r}_{\text{ph}} | \mathbf{q}, \mathbf{k} \rangle = e^{i\mathbf{q} \cdot \mathbf{r}_{\text{el}} + i\mathbf{k} \cdot \mathbf{r}_{\text{ph}}} / (2\pi)^3$, we can calculate the inner product in the above equation as

$$\begin{aligned} \langle \mathbf{r}_{\text{el}}, \mathbf{r}_{\text{ph}} | \Psi_{\text{sc}} \rangle &= \int \frac{d^3 q d^3 k}{(2\pi)^3} \psi_{\text{ini}}(\mathbf{q}_{\perp} + \mathbf{k}_{\perp}, q_z + \frac{ck}{v_z}) \sqrt{\Gamma(\mathbf{k})} e^{i\eta(\mathbf{k})} e^{i\mathbf{q} \cdot \mathbf{r}_{\text{el}} + i\mathbf{k} \cdot \mathbf{r}_{\text{ph}}} \\ &= \left(\frac{2}{\pi}\right)^{3/4} \Delta q_{\perp}^{\text{el}} (\Delta q_{\parallel}^{\text{el}})^{1/2} e^{-(\Delta q_{\perp}^{\text{el}})^2 |\mathbf{r}_{\perp}^{\text{el}}|^2 - (\Delta q_{\parallel}^{\text{el}})^2 z_{\text{el}}^2 + iq_0 z_{\text{el}}} \int \frac{d^3 k}{(2\pi)^{3/2}} \sqrt{\Gamma(\mathbf{k})} e^{-i\mathbf{k}_{\perp} \cdot (\mathbf{r}_{\perp}^{\text{el}} - \mathbf{r}_{\perp}^{\text{ph}})} e^{-i\frac{ck}{v_z} z_{\text{el}} + ik_z z_{\text{ph}}} e^{i\eta(\mathbf{k})}, \end{aligned} \quad (\text{C2})$$

where $\mathbf{r}_{\perp}^{\text{el}} = (x_{\text{el}}, y_{\text{el}})$ and $\mathbf{r}_{\perp}^{\text{ph}} = (x_{\text{ph}}, y_{\text{ph}})$. In the second equality, we have performed the integration over \mathbf{q} with Eqs. (5) and (6) for $\psi_{\text{ini}}(\mathbf{q})$. Therefore, Eq. (C1) yields

$$\begin{aligned} P(x_{\text{el}}, x_{\text{ph}}) &= \int dy_{\text{el}} dz_{\text{el}} dy_{\text{ph}} dz_{\text{ph}} \left(\frac{2}{\pi}\right)^{3/2} (\Delta q_{\perp}^{\text{el}})^2 \Delta q_{\parallel}^{\text{el}} e^{-2(\Delta q_{\perp}^{\text{el}})^2 |\mathbf{r}_{\perp}^{\text{el}}|^2 - 2(\Delta q_{\parallel}^{\text{el}})^2 z_{\text{el}}^2} \\ &\quad \times \int \frac{d^3 k d^3 k'}{(2\pi)^3} \sqrt{\Gamma(\mathbf{k}) \Gamma(\mathbf{k}')} e^{-i(\mathbf{k}_{\perp} - \mathbf{k}'_{\perp}) \cdot (\mathbf{r}_{\perp}^{\text{el}} - \mathbf{r}_{\perp}^{\text{ph}})} e^{-i\frac{c(k-k')}{v_z} z_{\text{el}} + i(k_z - k'_z) z_{\text{ph}}} e^{i[\eta(\mathbf{k}) - \eta(\mathbf{k}')] } \\ &= \frac{1}{2\pi} \left(\frac{2}{\pi}\right)^{3/2} (\Delta q_{\perp}^{\text{el}})^2 \Delta q_{\parallel}^{\text{el}} \int dy_{\text{el}} dz_{\text{el}} d^3 k d^3 k' e^{-2(\Delta q_{\perp}^{\text{el}})^2 |\mathbf{r}_{\perp}^{\text{el}}|^2 - 2(\Delta q_{\parallel}^{\text{el}})^2 z_{\text{el}}^2} \sqrt{\Gamma(\mathbf{k}) \Gamma(\mathbf{k}')} \\ &\quad \times \delta(k_y - k'_y) \delta(k_z - k'_z) e^{-i(\mathbf{k}_{\perp} - \mathbf{k}'_{\perp}) \cdot \mathbf{r}_{\perp}^{\text{el}}} e^{i(k_x - k'_x) x_{\text{ph}}} e^{-i\frac{c(k-k')}{v_z} z_{\text{el}}} e^{i[\eta(\mathbf{k}) - \eta(\mathbf{k}')] } \\ &= \frac{1}{2\pi} \left(\frac{2}{\pi}\right)^{3/2} (\Delta q_{\perp}^{\text{el}})^2 \Delta q_{\parallel}^{\text{el}} \int dy_{\text{el}} dz_{\text{el}} d^3 k dk'_x e^{-2(\Delta q_{\perp}^{\text{el}})^2 |\mathbf{r}_{\perp}^{\text{el}}|^2 - 2(\Delta q_{\parallel}^{\text{el}})^2 z_{\text{el}}^2} \sqrt{\Gamma(\mathbf{k}) \Gamma(k'_x, k_y, k_z)} \\ &\quad \times e^{-i(k_x - k'_x)(x_{\text{el}} - x_{\text{ph}})} e^{-i\frac{c}{v_z} (k - \sqrt{k_x'^2 + k_y^2 + k_z^2}) z_{\text{el}}} e^{i[\eta(\mathbf{k}) - \eta(k'_x, k_y, k_z)]}. \end{aligned} \quad (\text{C3})$$

In the second equality, we have used $\int dy e^{i(k_y - k'_y)y} = 2\pi \delta(k_y - k'_y)$. Furthermore by performing the integration over y_{el} and z_{el} , we obtain Eq. (20).

2. Joint wavevector distribution $P(q_x^{\text{el}}, k_x^{\text{ph}})$

We here derive Eq. (21) for the joint probability distribution $P(q_x^{\text{el}}, k_x^{\text{ph}})$ that the electron's wavevector is q_x^{el} and the photon's wavevector k_x^{ph} in the x direction.

The joint distribution $P(q_x^{\text{el}}, k_x^{\text{ph}})$ is defined by

$$P(q_x^{\text{el}}, k_x^{\text{ph}}) = \int dq_y^{\text{el}} dq_z^{\text{el}} dk_y^{\text{ph}} dk_z^{\text{ph}} |\langle \mathbf{q}^{\text{el}}, \mathbf{k}^{\text{ph}} | \Psi_{\text{sc}} \rangle|^2, \quad (\text{C4})$$

where $\mathbf{q}^{\text{el}} = (q_x^{\text{el}}, q_y^{\text{el}}, q_z^{\text{el}})$ and $\mathbf{k}^{\text{ph}} = (k_x^{\text{ph}}, k_y^{\text{ph}}, k_z^{\text{ph}})$. From Eqs. (2) and (3), we can calculate $P(\mathbf{q}^{\text{el}}, \mathbf{k}^{\text{ph}})$ as

$$P(\mathbf{q}^{\text{el}}, \mathbf{k}^{\text{ph}}) = |\psi_{\text{sc}}(\mathbf{q}^{\text{el}}, \mathbf{k}^{\text{ph}})|^2 = \left| \psi_{\text{ini}}(\mathbf{q}_{\perp}^{\text{el}} + \mathbf{k}_{\perp}^{\text{ph}}, q_z^{\text{el}} + \frac{ck^{\text{ph}}}{v_z}) \right|^2 \Gamma(\mathbf{k}^{\text{ph}}). \quad (\text{C5})$$

Substituting this into Eq. (C4) and performing the integration over q_y^{el} and q_z^{el} with the normalization conditions for $\psi_{\text{ini}}^{(y)}$ and $\psi_{\text{ini}}^{(z)}$, we obtain Eq. (21).

Appendix D: Calculation of the uncertainties

1. Relative position uncertainty $\langle [\Delta(x_{\text{el}} - x_{\text{ph}})]^2 \rangle$

We here derive Eqs. (14) and (16) for the relative position uncertainty $\langle [\Delta(x_{\text{el}} - x_{\text{ph}})]^2 \rangle$.

We first show that the average of $x_{\text{el}} - x_{\text{ph}}$ is zero. To this end, we note the relations $\Gamma(-k_x, k_y, k_z) = \Gamma(k_x, k_y, k_z)$ and $\eta(-k_x, k_y, k_z) = \eta(k_x, k_y, k_z)$, which follow from the in-plane rotational symmetry for $\Gamma(\mathbf{k})$ and $\eta(\mathbf{k})$. Equation (20) with these relations leads to $P(-x_{\text{el}}, -x_{\text{ph}}) = P(x_{\text{el}}, x_{\text{ph}})$. Therefore, $\langle x_{\text{el}} - x_{\text{ph}} \rangle = \int dx_{\text{el}} dx_{\text{ph}} P(x_{\text{el}}, x_{\text{ph}}) (x_{\text{el}} - x_{\text{ph}}) = 0$.

We then calculate the uncertainty $\langle [\Delta(x_{\text{el}} - x_{\text{ph}})]^2 \rangle = \langle (x_{\text{el}} - x_{\text{ph}})^2 \rangle$. From Eq. (20), we calculate it as

$$\begin{aligned}
\langle [\Delta(x_{\text{el}} - x_{\text{ph}})]^2 \rangle &= \int dx_{\text{el}} dx_{\text{ph}} P(x_{\text{el}}, x_{\text{ph}}) (x_{\text{el}} - x_{\text{ph}})^2 \\
&= \int dx_{\text{el}} dx_{\text{ph}} \frac{\Delta q_{\perp}^{\text{el}}}{\sqrt{2\pi^3}} e^{-2(\Delta q_{\perp}^{\text{el}})^2 x_{\text{el}}^2} \int d^3k dk'_x \sqrt{\Gamma(\mathbf{k})\Gamma(\mathbf{k}')} \left(-\frac{\partial^2}{\partial k_x'^2} e^{-i(k_x - k'_x)(x_{\text{el}} - x_{\text{ph}})} \right) e^{-c^2(k - k')^2 / [8v_z^2(\Delta q_{\parallel}^{\text{el}})^2]} e^{i[\eta(\mathbf{k}) - \eta(\mathbf{k}')] } \\
&= \int dx_{\text{el}} dx_{\text{ph}} d^3k dk'_x \frac{\Delta q_{\perp}^{\text{el}}}{\sqrt{2\pi^3}} e^{-2(\Delta q_{\perp}^{\text{el}})^2 x_{\text{el}}^2} e^{-i(k_x - k'_x)(x_{\text{el}} - x_{\text{ph}})} \left(-\frac{\partial^2}{\partial k_x'^2} \sqrt{\Gamma(\mathbf{k})\Gamma(\mathbf{k}')} e^{-c^2(k - k')^2 / [8v_z^2(\Delta q_{\parallel}^{\text{el}})^2]} e^{i[\eta(\mathbf{k}) - \eta(\mathbf{k}')] } \right) \\
&= \int dx_{\text{el}} d^3k dk'_x \frac{\Delta q_{\perp}^{\text{el}}}{\sqrt{2\pi^3}} 2\pi \delta(k_x - k'_x) e^{-2(\Delta q_{\perp}^{\text{el}})^2 x_{\text{el}}^2} \left(-\frac{\partial^2}{\partial k_x'^2} \sqrt{\Gamma(\mathbf{k})\Gamma(\mathbf{k}')} e^{-c^2(k - k')^2 / [8v_z^2(\Delta q_{\parallel}^{\text{el}})^2]} e^{i[\eta(\mathbf{k}) - \eta(\mathbf{k}')] } \right) \\
&= \int d^3k dk'_x \delta(k_x - k'_x) \left(-\frac{\partial^2}{\partial k_x'^2} \sqrt{\Gamma(\mathbf{k})\Gamma(\mathbf{k}')} e^{-c^2(k - k')^2 / [8v_z^2(\Delta q_{\parallel}^{\text{el}})^2]} e^{i[\eta(\mathbf{k}) - \eta(\mathbf{k}')] } \right) \\
&= \int d^3k \left\{ \frac{1}{4\Gamma(\mathbf{k})} \left(\frac{\partial \Gamma(\mathbf{k})}{\partial k_x} \right)^2 - \frac{1}{2} \frac{\partial^2 \Gamma(\mathbf{k})}{\partial k_x^2} + \frac{c^2 k_x^2}{4v_z^2(\Delta q_{\parallel}^{\text{el}})^2 k^2} \Gamma(\mathbf{k}) + \Gamma(\mathbf{k}) \left(\frac{\partial \eta(\mathbf{k})}{\partial k_x} \right)^2 \right\}. \tag{D1}
\end{aligned}$$

Furthermore, from the rotational symmetry in the transverse plane, we have

$$\langle [\Delta(x_{\text{el}} - x_{\text{ph}})]^2 \rangle = \langle [\Delta(y_{\text{el}} - y_{\text{ph}})]^2 \rangle = \frac{1}{2} \{ \langle [\Delta(x_{\text{el}} - x_{\text{ph}})]^2 \rangle + \langle [\Delta(y_{\text{el}} - y_{\text{ph}})]^2 \rangle \}. \tag{D2}$$

Since $\langle [\Delta(y_{\text{el}} - y_{\text{ph}})]^2 \rangle$ is obtained from Eq. (D1) by replacing k_x with k_y , the desired Eq. (14) follows from these relations.

Next, we assume the model for $\Gamma(\mathbf{k})$ [Eqs. (7)–(9)] and further evaluate $\langle [\Delta(x_{\text{el}} - x_{\text{ph}})]^2 \rangle$ in order to derive Eq. (16). To this end, we use the spherical coordinates ($k_x = k \sin \theta \cos \phi$, $k_y = k \sin \theta \sin \phi$, $k_z = k \cos \theta$ with the polar angle θ and azimuthal angle ϕ). We calculate the derivatives in Eq. (14) by noting $\partial \Gamma(\mathbf{k}) / \partial \phi = 0$ due to the rotational symmetry in the transverse plane. We then perform the integration in Eq. (14) to obtain

$$\begin{aligned}
&\frac{1}{8} \int d^3k \left\{ \frac{1}{\Gamma(\mathbf{k})} \left[\left(\frac{\partial \Gamma(\mathbf{k})}{\partial k_x} \right)^2 + \left(\frac{\partial \Gamma(\mathbf{k})}{\partial k_y} \right)^2 \right] - 2 \left(\frac{\partial^2 \Gamma(\mathbf{k})}{\partial k_x^2} + \frac{\partial^2 \Gamma(\mathbf{k})}{\partial k_y^2} \right) \right\} \\
&= \frac{15\mathcal{N}_g}{64\pi \Delta k_{\text{ph}}^4} \int_0^\infty dk \int_0^\pi d\theta \int_0^{2\pi} d\phi \sin \theta \cos^2 \theta e^{-(k - k_c)^2 / (2\Delta k_{\text{ph}}^2)} \left\{ -4\Delta k_{\text{ph}}^4 + 8\Delta k_{\text{ph}}^2 (k^2 - k_c k + 4\Delta k_{\text{ph}}^2) \sin^2 \theta \right. \\
&\quad \left. - \left[k^4 - 2k_c k^3 + (k_c^2 + 8\Delta k_{\text{ph}}^2) k^2 - 10k_c \Delta k_{\text{ph}}^2 k + 32\Delta k_{\text{ph}}^4 \right] \sin^4 \theta \right\} \\
&= \frac{\mathcal{N}_g \sqrt{2\pi}}{56} \left(19\Delta k_{\text{ph}} + \frac{2k_c^2}{\Delta k_{\text{ph}}} \right) \left[\text{erf} \left(\frac{k_c}{\sqrt{2}\Delta k_{\text{ph}}} \right) + 1 \right] + \frac{\mathcal{N}_g}{14} k_c \exp \left(-\frac{k_c^2}{2\Delta k_{\text{ph}}^2} \right), \tag{D3}
\end{aligned}$$

and

$$\frac{1}{8} \int d^3k \frac{c^2 k_{\perp}^2 \Gamma(\mathbf{k})}{v_z^2 (\Delta q_{\parallel}^{\text{el}})^2 k^2} = \frac{c^2}{8v_z^2 (\Delta q_{\parallel}^{\text{el}})^2} \int_0^\infty dk \int_0^\pi d\theta \int_0^{2\pi} d\phi k^2 \sin^3 \theta \Gamma(\mathbf{k}) = \frac{c^2}{14v_z^2 (\Delta q_{\parallel}^{\text{el}})^2}. \tag{D4}$$

We thus obtain Eq. (16).

2. Total wavevector uncertainty $\langle [\Delta(q_x^{\text{el}} + k_x^{\text{ph}})]^2 \rangle$

We here derive Eq. (15), $\langle [\Delta(q_x^{\text{el}} + k_x^{\text{ph}})]^2 \rangle = (\Delta q_{\perp}^{\text{el}})^2$, without assuming a model for $\Gamma(\mathbf{k})$.

We first show that the average of $q_x^{\text{el}} + k_x^{\text{ph}}$ is zero. Using Eqs. (21) and (5) and noting $|\psi_{\text{ini}}^{(x)}(-q_x)|^2 = |\psi_{\text{ini}}^{(x)}(q_x)|^2$, we calculate $\langle q_x^{\text{el}} + k_x^{\text{ph}} \rangle$ as

$$\begin{aligned}
\langle q_x^{\text{el}} + k_x^{\text{ph}} \rangle &= \int dq_x^{\text{el}} dk_x^{\text{ph}} P(q_x^{\text{el}}, k_x^{\text{ph}}) (q_x^{\text{el}} + k_x^{\text{ph}}) \\
&= \int dk_x^{\text{ph}} dk_y^{\text{ph}} dk_z^{\text{ph}} \Gamma(\mathbf{k}^{\text{ph}}) \int dq_x^{\text{el}} |\psi_{\text{ini}}^{(x)}(q_x^{\text{el}} + k_x^{\text{ph}})|^2 (q_x^{\text{el}} + k_x^{\text{ph}}) \\
&= 0. \tag{D5}
\end{aligned}$$

We then investigate the uncertainty $\langle [\Delta(q_x^{\text{el}} + k_x^{\text{ph}})]^2 \rangle = \langle (q_x^{\text{el}} + k_x^{\text{ph}})^2 \rangle$. Again, using Eqs. (21) and (5), we obtain the desired result:

$$\begin{aligned} \langle [\Delta(q_x^{\text{el}} + k_x^{\text{ph}})]^2 \rangle &= \int dq_x^{\text{el}} dk_x^{\text{ph}} P(q_x^{\text{el}}, k_x^{\text{ph}}) (q_x^{\text{el}} + k_x^{\text{ph}})^2 \\ &= \int dk_x^{\text{ph}} dk_y^{\text{ph}} dk_z^{\text{ph}} \Gamma(\mathbf{k}^{\text{ph}}) \int dq_x^{\text{el}} |\psi_{\text{ini}}^{(x)}(q_x^{\text{el}} + k_x^{\text{ph}})|^2 (q_x^{\text{el}} + k_x^{\text{ph}})^2 \\ &= (\Delta q_{\perp}^{\text{el}})^2. \end{aligned} \quad (\text{D6})$$

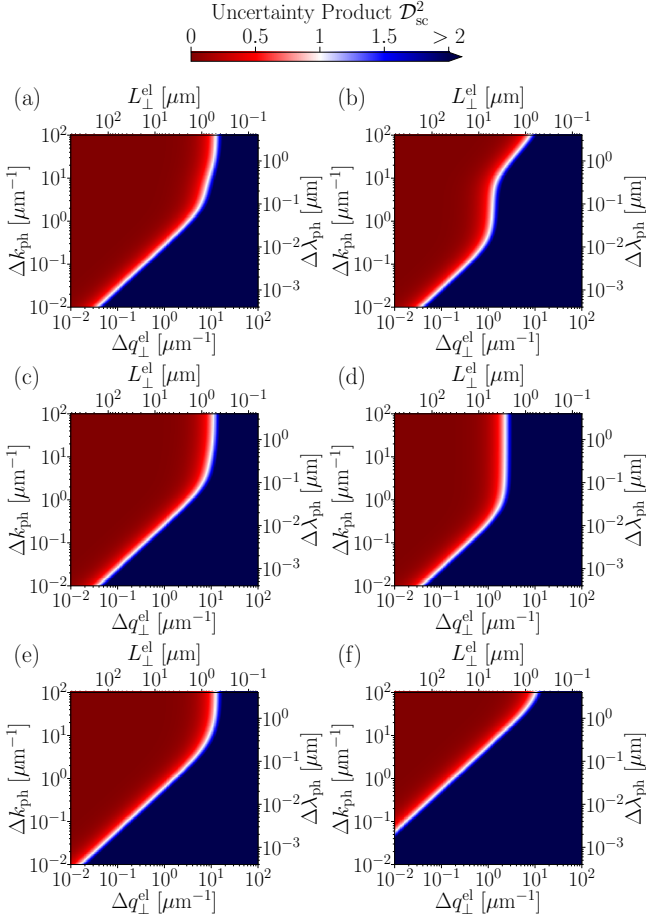


FIG. 7. Influence of the phase $\eta(\mathbf{k})$ on the uncertainty product $\mathcal{D}_{\text{sc}}^2$. Panels (a) and (b) correspond to the case where $\eta(\mathbf{k})$ depends only on θ and the additional term D_η is given by Eq. (E1) with $\xi_1 = 1$ for (a) and $\xi_1 = 100$ for (b). Panels (c) and (d) correspond to the case of $\eta_{21}(k) = \sqrt{\xi_2} k/k_c$ with $\xi_2 = 1$ for (c) and $\xi_2 = 100$ for (d). Panels (e) and (f) correspond to the case of $\eta_{22}(k) = \sqrt{\xi_2} k/\Delta k_{\text{ph}}$ with $\xi_2 = 1$ for (e) and $\xi_2 = 100$ for (f). The other parameter values are the same as those in Fig. 2.

Appendix E: Influence of the phase $\eta(\mathbf{k})$

In Sec. IV B, to discuss the entanglement intrinsic to the scattered state $|\Psi_{\text{sc}}\rangle$, we investigate the uncertainty

product $\mathcal{D}_{\text{sc}}^2$, focusing on the ideal case in which the phase-dependent term D_η vanishes in the relative position uncertainty $\langle [\Delta(x_{\text{el}} - x_{\text{ph}})]^2 \rangle$. However, in practical experiments, the condition $D_\eta = 0$ may not be perfectly achieved, and thus $\mathcal{D}_{\text{sc}}^2$ may appear to increase. In this appendix, we therefore investigate the influence of the phase $\eta(\mathbf{k})$ on $\mathcal{D}_{\text{sc}}^2$ by assuming several models for $\eta(\mathbf{k})$. We note that, while $\langle [\Delta(x_{\text{el}} - x_{\text{ph}})]^2 \rangle$ contains the phase-dependent term D_η , as seen in Eqs. (14) and (16), the total wavevector uncertainty $\langle [\Delta(q_x^{\text{el}} + k_x^{\text{ph}})]^2 \rangle$ is independent of the phase, as seen in Eq. (15).

We first consider the case where the phase $\eta(\mathbf{k})$ depends only on the polar angle θ , i.e., $\eta(\mathbf{k}) = \eta_1(\theta)$. In this case, D_η reduces to

$$D_{\eta_1} = \xi_1 \sqrt{\frac{\pi}{2}} \mathcal{N}_g \Delta k_{\text{ph}} \left[\text{erf} \left(\frac{k_c}{\sqrt{2} \Delta k_{\text{ph}}} \right) + 1 \right], \quad (\text{E1})$$

where the dimensionless factor ξ_1 is defined as

$$\xi_1 = \pi \int_0^\pi d\theta \sin \theta \cos^2 \theta f(\theta) \left(\frac{\partial \eta_1(\theta)}{\partial \theta} \right)^2, \quad (\text{E2})$$

with $f(\theta)$ given by Eq. (9). For example, $\xi_1 = 3/14$ when $\eta_1(\theta) = \theta$.

Figures 7(a) and (b) show color plots of $\mathcal{D}_{\text{sc}}^2$ for this case with $\xi_1 = 1$ and $\xi_1 = 100$, respectively. Compared with Fig. 2(c), the result for $\xi_1 = 1$ remains nearly unchanged, whereas a clear deviation appears for $\xi_1 = 100$ in the large- Δk_{ph} regime. This behavior can be understood from the relation between D_{η_1} and the term

$$D_0 = \frac{19\sqrt{2}\pi}{56} \mathcal{N}_g \Delta k_{\text{ph}} \left[\text{erf} \left(\frac{k_c}{\sqrt{2} \Delta k_{\text{ph}}} \right) + 1 \right], \quad (\text{E3})$$

which appears in $\langle [\Delta(x_{\text{el}} - x_{\text{ph}})]^2 \rangle$ [Eq. (16)]. Since $D_{\eta_1} \propto \xi_1 D_0$, its relative importance is controlled by ξ_1 . For $\xi_1 \lesssim 1$, one has $D_{\eta_1} \lesssim D_0$, so its contribution to $\langle [\Delta(x_{\text{el}} - x_{\text{ph}})]^2 \rangle$ is minor and $\mathcal{D}_{\text{sc}}^2$ remains essentially unchanged. In contrast, for $\xi_1 \gg 1$, D_{η_1} dominates at large Δk_{ph} , leading to $\mathcal{D}_{\text{sc}}^2 \simeq D_{\eta_1} (\Delta q_{\perp}^{\text{el}})^2$. Furthermore, around $\Delta k_{\text{ph}} \approx k_c$, the dependence of D_{η_1} on Δk_{ph} is weak, so the contour $\mathcal{D}_{\text{sc}}^2 = 1$ becomes nearly vertical in the $\Delta q_{\perp}^{\text{el}} - \Delta k_{\text{ph}}$ plane. For $\Delta k_{\text{ph}} \gg k_c$, $D_{\eta_1} \propto 1/\Delta k_{\text{ph}}^2$, which implies $\Delta q_{\perp}^{\text{el}} \propto \Delta k_{\text{ph}}$ along the $\mathcal{D}_{\text{sc}}^2 = 1$ contour for sufficiently large Δk_{ph} .

We next consider the case where the phase $\eta(\mathbf{k})$ depends only on $k = |\mathbf{k}|$, i.e., $\eta(\mathbf{k}) = \eta_2(k)$. In this case, D_η reduces to

$$D_{\eta_2} = \frac{2}{7} \int_0^\infty dk k^2 g(k) \left(\frac{\partial \eta_2(k)}{\partial k} \right)^2, \quad (\text{E4})$$

where $g(k)$ is given by Eq. (8). Since $\eta_2(k)$ is dimensionless, it may be a function of k/k_c and $k/\Delta k_{\text{ph}}$. As minimal models, we consider $\eta_{21}(k) = \sqrt{\xi_2} k/k_c$ and $\eta_{22}(k) = \sqrt{\xi_2} k/\Delta k_{\text{ph}}$ with a dimensionless constant ξ_2 . These models yield $D_{\eta_{21}} = 2\xi_2/(7k_c^2)$ and $D_{\eta_{22}} = 2\xi_2/(7\Delta k_{\text{ph}}^2)$, respectively.

Figures 7(c) and (d) show color plots of $\mathcal{D}_{\text{sc}}^2$ for $\eta_{21}(k) = \sqrt{\xi_2} k/k_c$ with $\xi_2 = 1$ and $\xi_2 = 100$, respectively. Compared with Fig. 2(c), the result for $\xi_2 = 1$ is nearly unchanged, whereas for $\xi_2 = 100$ the vertical segment of the $\mathcal{D}_{\text{sc}}^2 = 1$ contour becomes longer and shifts

to smaller Δk_{ph} . This behavior can be understood from the fact that $D_{\eta_{21}} = 2\xi_2/(7k_c^2)$ is independent of Δk_{ph} , whereas the other contributions to $\langle [\Delta(x_{\text{el}} - x_{\text{ph}})]^2 \rangle$ either decrease or remain unchanged as Δk_{ph} increases. As a result, for large Δk_{ph} and $\xi \gg 1$, $D_{\eta_{21}}$ becomes the dominant contribution. Moreover, a larger ξ_2 accelerates this crossover to the $D_{\eta_{21}}$ -dominated regime. In this regime, one finds $\mathcal{D}_{\text{sc}}^2 \propto \xi_2 (\Delta q_{\perp}^{\text{el}})^2$, so that the contour $\mathcal{D}_{\text{sc}}^2 = 1$ becomes nearly vertical in the $\Delta q_{\perp}^{\text{el}} - \Delta k_{\text{ph}}$ plane, as seen in Fig. 7(d).

Figures 7(e) and (f) show color plots of $\mathcal{D}_{\text{sc}}^2$ for $\eta_{22}(k) = \sqrt{\xi_2} k/\Delta k_{\text{ph}}$ with $\xi_2 = 1$ and $\xi_2 = 100$, respectively. Compared with Fig. 2(c), the $\mathcal{D}_{\text{sc}}^2 = 1$ contour shifts upward as ξ_2 increases. This behavior follows directly from the form of $D_{\eta_{22}} = 2\xi_2/(7\Delta k_{\text{ph}}^2)$, which enhances the contribution ($\propto 1/\Delta k_{\text{ph}}^2$) in $\langle [\Delta(x_{\text{el}} - x_{\text{ph}})]^2 \rangle$ at small Δk_{ph} for larger ξ_2 .

-
- [1] A. Tonomura, N. Osakabe, T. Matsuda, T. Kawasaki, J. Endo, S. Yano, and H. Yamada, Evidence for Aharonov-Bohm effect with magnetic field completely shielded from electron wave, *Phys. Rev. Lett.* **56**, 792 (1986).
- [2] A. Tonomura, J. Endo, T. Matsuda, T. Kawasaki, and H. Ezawa, Demonstration of single-electron buildup of an interference pattern, *American Journal of Physics* **57**, 117 (1989).
- [3] R. Ruimy, A. Karnieli, and I. Kaminer, Free-electron quantum optics, *Nature Physics* **21**, 193 (2025).
- [4] F. J. García de Abajo, A. Polman, C. I. Velasco, M. Kociak, L. H. G. Tizei, O. Stéphan, S. Meuret, T. Sannomiya, K. Akiba, Y. Auad, A. Feist, C. Ropers, P. Baum, J. H. Gaida, M. Siviš, H. Lourenço-Martins, L. Serafini, J. Verbeeck, A. Konečná, N. Talebi, B. M. Ferrari, C. J. R. Duncan, M. G. Bravi, I. Ostroman, G. M. Vanacore, E. Nussinson, R. Ruimy, Y. Adiv, A. Niedermayr, I. Kaminer, V. Di Giulio, O. Kfir, Z. Zhao, R. Shiloh, Y. Morimoto, M. Kozák, P. Hommelhoff, F. Barantani, F. Carbone, F. Shahshouri, W. Albrecht, S. Rey, T. Coenen, E. Kieft, H. L. Lalande Robert, F. de Jong, and M. Solà-Garcia, Roadmap for quantum nanophotonics with free electrons, *ACS Photonics* **12**, 4760 (2025).
- [5] V. Giovannetti, S. Lloyd, and L. Maccone, Quantum-enhanced measurements: Beating the standard quantum limit, *Science* **306**, 1330 (2004).
- [6] V. Giovannetti, S. Lloyd, and L. Maccone, Advances in quantum metrology, *Nature Photonics* **5**, 222 (2011).
- [7] C. L. Degen, F. Reinhard, and P. Cappellaro, Quantum sensing, *Rev. Mod. Phys.* **89**, 035002 (2017).
- [8] M. Barbieri, Optical quantum metrology, *PRX Quantum* **3**, 010202 (2022).
- [9] M. A. Nielsen and I. L. Chuang, *Quantum Computation and Quantum Information* (Cambridge University Press, Cambridge; New York, 2010).
- [10] Y. Yamamoto and K. Semba, eds., *Principles and Methods of Quantum Information Technologies* (Springer Tokyo, 2016).
- [11] M. M. Wilde, *Quantum Information Theory*, 2nd ed. (Cambridge University Press, Cambridge; New York, 2017).
- [12] C. Mechel, Y. Kurman, A. Karnieli, N. Rivera, A. Arie, and I. Kaminer, Quantum correlations in electron microscopy, *Optica* **8**, 70 (2021).
- [13] C. Roques-Carmes, S. E. Kooi, Y. Yang, N. Rivera, P. D. Keathley, J. D. Joannopoulos, S. G. Johnson, I. Kaminer, K. K. Berggren, and M. Soljačić, Free-electron-light interactions in nanophotonics, *Applied Physics Reviews* **10**, 011303 (2023).
- [14] B. Barwick, D. J. Flannigan, and A. H. Zewail, Photon-induced near-field electron microscopy, *Nature* **462**, 902 (2009).
- [15] A. Feist, K. E. Echterkamp, J. Schauss, S. V. Yalunin, S. Schäfer, and C. Ropers, Quantum coherent optical phase modulation in an ultrafast transmission electron microscope, *Nature* **521**, 200 (2015).
- [16] O. Kfir, Entanglements of electrons and cavity photons in the strong-coupling regime, *Phys. Rev. Lett.* **123**, 103602 (2019).
- [17] O. Kfir, V. D. Giulio, F. J. G. de Abajo, and C. Ropers, Optical coherence transfer mediated by free electrons, *Science Advances* **7**, eabf6380 (2021).
- [18] A. Karnieli, N. Rivera, A. Arie, and I. Kaminer, The coherence of light is fundamentally tied to the quantum coherence of the emitting particle, *Science Advances* **7**, eabf8096 (2021).
- [19] Y. Pan and A. Gover, Beyond Fermi's golden rule in free-electron quantum electrodynamics: acceleration/radiation correspondence, *New Journal of Physics* **23**, 063070 (2021).
- [20] A. Konečná, F. Iyikanat, and F. J. G. de Abajo, Entangling free electrons and optical excitations, *Science Advances* **8**, eabo7853 (2022).
- [21] G. Huang, N. J. Engelsen, O. Kfir, C. Ropers, and T. J. Kippenberg, Electron-photon quantum state heralding using photonic integrated circuits, *PRX Quantum* **4**, 020351 (2023).
- [22] E. Kazakevich, H. Aharon, and O. Kfir, Spatial electron-

- photon entanglement, *Phys. Rev. Res.* **6**, 043033 (2024).
- [23] X. Shi, L. W. W. Wong, S. Huang, L. J. Wong, and I. Kaminer, Transverse recoil imprinted on free-electron radiation, *Nature Communications* **15**, 7803 (2024).
- [24] J.-W. Henke, H. Jeng, and C. Ropers, Probing electron-photon entanglement using a quantum eraser, *Phys. Rev. A* **111**, 012610 (2025).
- [25] P. Rembold, S. Beltrán-Romero, A. Preimesberger, S. Bogdanov, I. C. Bicket, N. Friis, E. Agudelo, D. Rätzel, and P. Haslinger, State-agnostic approach to certifying electron–photon entanglement in electron microscopy, *Quantum Science and Technology* **10**, 045003 (2025).
- [26] A. Feist, G. Huang, G. Arend, Y. Yang, J.-W. Henke, A. S. Raja, F. J. Kappert, R. N. Wang, H. Lourenço-Martins, Z. Qiu, J. Liu, O. Kfir, T. J. Kippenberg, and C. Ropers, Cavity-mediated electron-photon pairs, *Science* **377**, 777 (2022).
- [27] A. Preimesberger, D. Hornof, T. Dorfner, T. Schachinger, M. Hrtoň, A. Konečná, and P. Haslinger, Exploring single-photon recoil on free electrons, *Phys. Rev. Lett.* **134**, 096901 (2025).
- [28] A. Preimesberger, S. Bogdanov, I. C. Bicket, P. Rembold, and P. Haslinger, *Experimental verification of electron-photon entanglement* (2025), [arXiv:2504.13163 \[quant-ph\]](https://arxiv.org/abs/2504.13163).
- [29] J.-W. Henke, H. Jeng, M. Sivis, and C. Ropers, *Observation of quantum entanglement between free electrons and photons* (2025), [arXiv:2504.13047 \[quant-ph\]](https://arxiv.org/abs/2504.13047).
- [30] H. Okamoto and Y. Nagatani, Entanglement-assisted electron microscopy based on a flux qubit, *Applied Physics Letters* **104**, 062604 (2014).
- [31] P. Kruit, R. Hobbs, C.-S. Kim, Y. Yang, V. Manfrinato, J. Hammer, S. Thomas, P. Weber, B. Klopfer, C. Kohstall, T. Juffmann, M. Kasevich, P. Hommelhoff, and K. Berggren, Designs for a quantum electron microscope, *Ultramicroscopy* **164**, 31 (2016).
- [32] C. I. Velasco and F. J. García de Abajo, Quantum sensing and metrology with free electrons, *Nature Communications* **17**, 868 (2025).
- [33] O. Reinhardt, C. Mechel, M. Lynch, and I. Kaminer, Free-electron qubits, *Annalen der Physik* **533**, 2000254 (2021).
- [34] A. Karnieli, S. Tsesses, R. Yu, N. Rivera, A. Arie, I. Kaminer, and S. Fan, Universal and ultrafast quantum computation based on free-electron-polariton blockade, *PRX Quantum* **5**, 010339 (2024).
- [35] N. Talebi, Strong interaction of slow electrons with near-field light visited from first principles, *Phys. Rev. Lett.* **125**, 080401 (2020).
- [36] Z. Xie, Z. Chen, H. Li, Q. Yan, H. Chen, X. Lin, I. Kaminer, O. D. Miller, and Y. Yang, Maximal quantum interaction between free electrons and photons, *Phys. Rev. Lett.* **134**, 043803 (2025).
- [37] Z. Zhao, Upper bound for the quantum coupling between free electrons and photons, *Phys. Rev. Lett.* **134**, 043804 (2025).
- [38] F. J. García de Abajo, Optical excitations in electron microscopy, *Rev. Mod. Phys.* **82**, 209 (2010).
- [39] F. J. García de Abajo and V. Di Giulio, Optical excitations with electron beams: Challenges and opportunities, *ACS Photonics* **8**, 945 (2021).
- [40] S. Mancini, V. Giovannetti, D. Vitali, and P. Tombesi, Entangling macroscopic oscillators exploiting radiation pressure, *Phys. Rev. Lett.* **88**, 120401 (2002).
- [41] D. B. Williams and C. B. Carter, *Transmission Electron Microscopy* (Springer New York, NY, 2009).
- [42] R. Grobe, K. Rzazewski, and J. H. Eberly, Measure of electron-electron correlation in atomic physics, *Journal of Physics B: Atomic, Molecular and Optical Physics* **27**, L503 (1994).
- [43] K. W. Chan, C. K. Law, and J. H. Eberly, Localized single-photon wave functions in free space, *Phys. Rev. Lett.* **88**, 100402 (2002).
- [44] K. W. Chan, C. K. Law, and J. H. Eberly, Quantum entanglement in photon-atom scattering, *Phys. Rev. A* **68**, 022110 (2003).
- [45] C. K. Law and J. H. Eberly, Analysis and interpretation of high transverse entanglement in optical parametric down conversion, *Phys. Rev. Lett.* **92**, 127903 (2004).
- [46] M. V. Fedorov, M. A. Efremov, A. E. Kazakov, K. W. Chan, C. K. Law, and J. H. Eberly, Spontaneous emission of a photon: Wave-packet structures and atom-photon entanglement, *Phys. Rev. A* **72**, 032110 (2005).
- [47] R. Guo and H. Guo, Entanglement of a scattered single photon with an atom, *Phys. Rev. A* **73**, 012103 (2006).
- [48] R. Guo and H. Guo, Momentum entanglement and disentanglement between an atom and a photon, *Phys. Rev. A* **76**, 012112 (2007).
- [49] H. Di Lorenzo Pires, C. H. Monken, and M. P. van Exter, Direct measurement of transverse-mode entanglement in two-photon states, *Phys. Rev. A* **80**, 022307 (2009).
- [50] A. D’Errico and E. Karimi, Imaging of biphoton states: Fundamentals and applications, *Advanced Functional Materials*, e26562 (2026).
- [51] J. C. Howell, R. S. Bennink, S. J. Bentley, and R. W. Boyd, Realization of the Einstein-Podolsky-Rosen paradox using momentum- and position-entangled photons from spontaneous parametric down conversion, *Phys. Rev. Lett.* **92**, 210403 (2004).
- [52] M. D’Angelo, A. Valencia, M. H. Rubin, and Y. Shih, Resolution of quantum and classical ghost imaging, *Phys. Rev. A* **72**, 013810 (2005).
- [53] S. Walborn, C. Monken, S. Pádua, and P. Souto Ribeiro, Spatial correlations in parametric down-conversion, *Physics Reports* **495**, 87 (2010).